

Winter 2011

Studies of net community productivity in a near-coastal temperate ecosystem

Olivia De Meo

University of New Hampshire, Durham

Follow this and additional works at: <https://scholars.unh.edu/thesis>

Recommended Citation

De Meo, Olivia, "Studies of net community productivity in a near-coastal temperate ecosystem" (2011). *Master's Theses and Capstones*. 682.

<https://scholars.unh.edu/thesis/682>

This Thesis is brought to you for free and open access by the Student Scholarship at University of New Hampshire Scholars' Repository. It has been accepted for inclusion in Master's Theses and Capstones by an authorized administrator of University of New Hampshire Scholars' Repository. For more information, please contact nicole.hentz@unh.edu.

**STUDIES OF NET COMMUNITY
PRODUCTIVITY IN A NEAR-COASTAL
TEMPERATE ECOSYSTEM**

BY

OLIVIA DE MEO

Bachelor of Arts, Illinois Wesleyan University, 2009

THESIS

Submitted to the University of New Hampshire
in partial fulfillment of
the requirements for the Degree of

Master of Science

in

Earth Sciences – Oceanography

December 2011

UMI Number: 1507820

All rights reserved

INFORMATION TO ALL USERS

The quality of this reproduction is dependent upon the quality of the copy submitted.

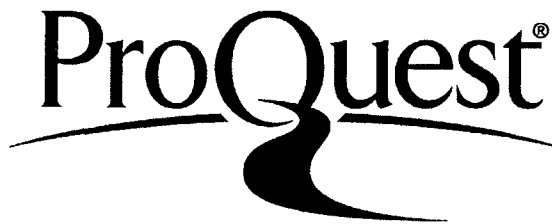
In the unlikely event that the author did not send a complete manuscript and there are missing pages, these will be noted. Also, if material had to be removed, a note will indicate the deletion.



UMI 1507820

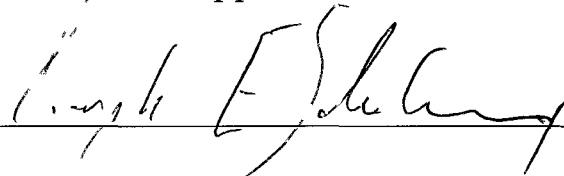
Copyright 2012 by ProQuest LLC.

All rights reserved. This edition of the work is protected against unauthorized copying under Title 17, United States Code.



ProQuest LLC
789 East Eisenhower Parkway
P.O. Box 1346
Ann Arbor, MI 48106-1346

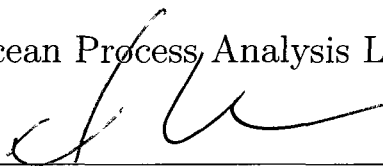
This thesis has been examined and approved.



Thesis Advisor: Joseph Salisbury

Research Assistant Professor

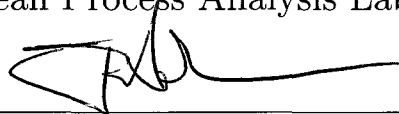
Ocean Process Analysis Lab



Doug Vandemark

Research Associate Professor

Ocean Process Analysis Lab



Tim Moore

Research Scientist

Ocean Process Analysis Lab

8 Dec 2011

Date

TABLE OF CONTENTS

LIST OF TABLES	v
LIST OF FIGURES	vi
ABSTRACT	viii
1 INTRODUCTION	1
1.1 Objectives	3
1.2 Background	4
1.2.1 Methods of NCP Measurement	4
1.2.2 Relationship of NCP to Air-Sea Flux	6
1.2.3 Causes of Variability in Coastal NCP	8
1.2.4 Optical Parameters for Estimation of NCP	9
2 DRIFTER STUDY	14
2.1 Site Description	14
2.2 Methods	15
2.2.1 Sample Collection and Analysis	15
2.2.2 Data Processing	17
2.3 Results	22
2.3.1 Hydrography	22
2.3.2 Oxygen Corrections	22
2.3.3 Net Community Productivity	24
2.3.4 Optical Proxies for NCP	24
2.4 Discussion	26
2.4.1 Sources of Error	27

2.4.2	Net Community Productivity	30
2.4.3	Optical Proxy Relationships	31
2.4.4	Experiment Weaknesses	32
2.4.5	Improvements for Future Experiments	34
2.4.6	Implications and Conclusions	35
3	INCUBATION STUDY	48
3.1	Site Description	48
3.2	Methods	49
3.2.1	Data Collection	49
3.2.2	Data Processing	51
3.3	Results	51
3.4	Discussion	53
3.4.1	Initial Problems	53
3.4.2	GPP, Respiration, and NCP Rates	53
3.4.3	No Production	54
3.4.4	Dark Production	55
3.4.5	PAR Pattern	56
3.5	Improvements and Future Experiments	56
4	CONCLUSION	67
	REFERENCES	69

List of Tables

2.1	NCP _{OC} error table	46
2.2	NCP _{O₂} error table	47

List of Figures

1-1	Biological Pump	13
2-1	Oxygen corrections	38
2-2	Chlorophyll corrections	38
2-3	POC regressions	38
2-4	Temperature	39
2-5	Salinity	39
2-6	Fluorescent chlorophyll	40
2-7	Biological oxygen anomaly	40
2-8	Schmidt number time series	41
2-9	10 m wind speed time series	41
2-10	Piston velocity time series	41
2-11	Air-sea flux time series	41
2-12	Bubble injection time series	42
2-13	Diffusion time series	42
2-14	NCP_{O_2} time series	42
2-15	$NCP_{OC}(chl-a)$ vs. NCP_{O_2} over the day	43
2-16	$NCP_{OC}(chl-a)$ vs. NCP_{O_2} between casts	43
2-17	$NCP_{OC}(f-chl)$ vs. NCP_{O_2} over the day	43
2-18	$NCP_{OC}(f-chl)$ vs. NCP_{O_2} between casts	43
2-19	$NCP_{OC}(c_p)$ vs. NCP_{O_2} over the day	44
2-20	$NCP_{OC}(c_p)$ vs. NCP_{O_2} between casts	44
2-21	Δ Depth-Integrated c_p vs. NCP_{O_2} over the day	44

2-22	Δ Depth-Integrated c_p vs. NCP_{O_2} between casts	44
2-23	$NCP_{OC}(b_{bp})$ vs. NCP_{O_2} over the day	45
2-24	$NCP_{OC}(b_{bp})$ vs. NCP_{O_2} between casts	45
3-1	Piscataqua Estuary Inlet	58
3-2	Tank	59
3-3	Incubation Chamber	59
3-4	Settling Chamber	60
3-5	Expected Δ Biological Oxygen	61
3-6	Expected Δ Temperature	61
3-7	Expected PAR	62
3-8	No production biological oxygen	62
3-9	No production temperature	63
3-10	No production PAR	63
3-11	Dark production biological oxygen	64
3-12	Dark Production temperature	64
3-13	Dark production PAR	65
3-14	GPP, respiration, and NCP rates	66

ABSTRACT

STUDIES OF NET COMMUNITY PRODUCTIVITY IN A NEAR-COASTAL TEMPERATE ECOSYSTEM

by

Olivia De Meo

University of New Hampshire, December, 2011

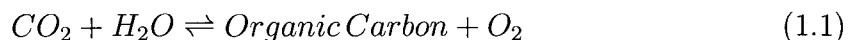
Understanding the biological contribution to the carbon cycle is important to accurately calculate oceanic carbon budgets. The biological contribution to air-sea flux can be expressed as net community productivity (NCP), or the difference between gross primary production and community respiration. This study conducted two experiments to constrain NCP in a near-coastal region. The first experiment conducted in the western Gulf of Maine (GoM) sought to identify an indirect optical proxy for NCP that would allow for the determination of NCP remotely by satellite in the future. NCP results indicated that the GoM was near equilibrium during our study. Changes in particulate organic carbon inventory derived from beam attenuation proved to be the most robust proxy of NCP. The second experiment evaluated a novel custom-built autonomous incubation instrument for continuous NCP and respiration measurement in the Piscataqua Estuary Inlet. Although some questionable data patterns were occasionally observed, NCP and respiration rates correlated well with the literature where good data was recorded.

CHAPTER 1

INTRODUCTION

The coastal zone accounts for only about 7% of the ocean's surface area (Borges, 2011), but despite its small size, it is one of the most biogeochemically active regions and plays an important role in the carbon cycle. Riverine inputs and upwelling transport organic carbon and nutrients conducive to significant biological productivity, which stimulates the export of carbon to the deep ocean through a mechanism known as the biological pump (Fig. 1-1). Thus, quantifying the coastal ocean's role in the carbon cycle has become an important consideration for calculating oceanic carbon budgets.

Net community productivity (NCP), defined as the difference between gross primary productivity (GPP) and community respiration (R), is an important indicator of the role of the biota in sequestering and exporting carbon. NCP is related to the production and consumption of carbon by the general equation,



where the forward form of the equation represents photosynthesis and the reverse is respiration. It is evident from equation 1.1 that NCP can be tracked by changes in dissolved inorganic carbon (DIC) and dissolved oxygen (DO). Odum (1956) was the first to use DO to study NCP as the basis for classifying communities as net autotrophic ($GPP > R$) or net heterotrophic ($GPP < R$). Consequently, based on these classifications, NCP is a useful tool for understanding the biological component of carbon cycling by determining whether a coastal community is a source or sink of CO_2 .

Debate exists over the role of the coastal ocean in the global carbon cycle. Several studies have shown that coastal margin systems are a net source of CO₂ (Frankignoulle et al., 1998; Cai et al., 2003), while others have shown them to sequester carbon (Borges and Frankignoulle, 2002; Kortzinger, 2003; Thomas et al., 2004). It will be difficult to resolve this debate until more is known about coastal carbon dynamics. Unfortunately, the coastal region is difficult to characterize due to its complex interactions with the land, atmosphere, and open ocean. These interactions are further complicated by anthropogenic effects. Coastal areas are particularly sensitive to anthropogenic perturbations of the land, which affect the timing, magnitude, and concentrations of organic matter and nutrient deposition by rivers (Hopkinson and Vallino, 1995). Thus, human-induced changes to coastal organic carbon loading can alter the balance of carbon in the system and affect heterotrophic processes, while nutrient inputs can stimulate production.

Furthermore, it is estimated that from 1850 to 1996, anthropogenic fossil fuel use emitted roughly 340 Pg of carbon to the atmosphere, nearly 30% of which has dissolved into the oceans (Falkowski and Raven, 2007). These emissions of CO₂, a potent greenhouse gas, are predicted to cause temperatures to rise, resulting in a more stratified water column (Falkowski et al., 2003). This decreases the ability of deep water to mix up to the surface and bring with it nutrients, reducing primary productivity. Additionally, rising temperatures could alter oceanic circulation patterns and affect upwelling (Falkowski et al., 2003), the primary driver of coastal biological activity (Libes, 1992). These effects on biological activity could alter the biological pump and therefore the ocean's ability to sequester carbon.

It is important then to gain a better understanding of NCP and its effects on carbon cycling as well as to be able to monitor changes in the future. This research will present the first steps taken to identify a proxy for remote retrieval of NCP by satellite, which has the potential to aid in future global estimations of NCP. Additionally, this

study seeks to gain a better understanding of NCP through long-term monitoring with a novel incubation instrument in the hopes of aggregating a large data set of gross production, community respiration, and net community production.

1.1 Objectives

This research consisted of two experiments. The purpose of the first experiment was two-fold. The first goal of this study was to gain a better understanding of carbon cycling in the coastal zone by observing the timing and magnitude of NCP in the western Gulf of Maine (GoM) while tracking a drifter over the course of two weeks. The second goal was to use the data collected on the cruises to identify an optical parameter that would act as an indirect index for NCP and potentially allow for remote retrieval of NCP by satellite. We hypothesize that NCP, measured as the temporal derivative of the biological oxygen inventory will be tracked by changes in the particulate organic carbon (POC) inventory, which can be sufficiently estimated from optical parameters. To that end, we examined chlorophyll-*a* (*chl-a*), particle attenuation at 660 nm ($c_p(660)$), and particle backscattering at 555 nm ($b_{bp}(555)$) as estimators of POC. This research is important because *in situ* ship-sampling is expensive and only provides sparse regional data that are of little use in calculating a global carbon budget. However, satellites provide access to global data sets. If one or more of these optical parameters is found to be a good proxy for NCP, then NCP can be constrained globally through the use of satellite ocean-color products and the existing global carbon budget can be improved.

The goal of the second experiment was to determine NCP in the Piscataqua Estuary Inlet and build a large data base of production and respiration rates. We hypothesize that NCP will vary seasonally with changes in nutrient supply, organic carbon, and light. Additionally, we expect to see a year-round tidal signal as freshwater en-

ters via the Piscataqua River and different NCP signals from varying phytoplankton communities. In an effort to improve field methods, this experiment utilized a novel instrument created by Langdon Enterprises (Miami, FL) that automatically incubates seawater in light and dark chambers while simultaneously measuring changes in dissolved oxygen, which can be used to calculate NCP. This research is poised to build upon existing knowledge of coastal carbon cycling by providing a long-term data set of NCP. Furthermore, little respiration data exist and current models often assume respiration to be constant. Respiration rates in this experiment were calculated from the dark chamber incubations. As a result, this study provides a long-term data set of respiration rates during both daytime and nighttime hours.

1.2 Background

1.2.1 Methods of NCP Measurement

The development of methods to measure NCP began as early as the 1920s when Gaarder and Gran (1927) first developed light and dark oxygen incubations. With this technique, oxygen concentrations are measured at the beginning and end of the incubation using the Winkler titration method. Net community productivity is measured in the light bottles and respiration is measured in the dark bottles. Similarly, the rate of change in carbon dioxide can also be measured. Smith and Marsh (1973) examined whether changes in oxygen or carbon dioxide gave a better estimate of organic carbon production in coral reefs and found good agreement using both measurements. Another incubation approach developed by Steemann-Nielsen (1952) involved the use of ^{14}C as a radiotracer, which could measure the amount of carbon fixed when a bottle of seawater was incubated at depth. This method became the preferred method of measurement, but it does not provide any respiration data so our knowledge of respiration and therefore the balance of carbon that is exportable, remains poor. Much

confusion ensued over the years about what the ^{14}C method actually measured, and it is now thought to measure a rate in between gross and net production. Both light/dark and ^{14}C incubation approaches suffer from bottle effects because removing organisms from the ocean environment and sequestering them in a bottle reduces the variability that they experience in real seawater (Marra, 2002).

A method that avoids bottle effects is the open-water oxygen method, developed by Odum (1956), in which oxygen sensors are placed *in situ* to measure DO. The data are later corrected for air-sea gas exchange, so NCP depends strongly on which gas transfer parameterization is employed (Gazeau et al., 2005). An additional alternative that avoids bottle effects is to compare O_2 measurements to an abiotic gas. Abiotic gases give an account of the physical forcings that have occurred and are not affected by biological activity like O_2 . The abiotic gas chosen must have similar diffusivity and solubility coefficients as O_2 so that it equilibrates with the atmosphere on the same timescale. For this reason, Ar or N_2 are usually chosen. NCP can then be calculated as the difference between O_2 and Ar or N_2 over the time needed to equilibrate with the atmosphere (McNeil et al., 2006a). While these field methods provide good local *in situ* data, they are not feasible for gathering global NCP data.

In an effort to calculate NCP across large spatial and temporal scales, several budgeting approaches have also been taken. The first is the construction of a DIC budget, which relies on knowledge of air-sea flux and measurements of DIC to solve for NCP. However, an assumption of the DIC budget method is that only DIC input/output, air-sea flux, and biological production and consumption affect DIC concentrations; precipitation and dissolution of CaCO_3 are not considered (Gazeau et al., 2005). Another budgeting approach is the Land Ocean Interaction in the Coastal Zone (LOICZ) stoichiometry budget. This budget is based on non-conservative fluxes of dissolved inorganic phosphorus (DIP). However, this method assumes that dissolved organic phosphorus (DOP) fluxes are inconsequential, DIP fluxes are only due to pelagic bi-

ological activity, and a Redfield ratio to convert DIP to carbon units (Gazeau et al., 2005). The validity of budgeting approaches versus incubation measurements was assessed by Gazeau et al. (2005). They found that each method had limitations, but all generally converged on similar estimates.

Several more methods have been used to estimate global NCP. Lee (2001) calculated NCP in the surface mixed layer through two approaches. The first was an approximation from the change in salinity-normalized total DIC inventory, which was corrected for air-sea flux and diffusion. The second approach employed a thermodynamic model with monthly mean $p\text{CO}_2$ and total alkalinity. Both showed good agreement with an annual NCP of 9.1 ± 2.7 and 10.8 ± 2.7 Pg C yr^{-1} respectively. Alternatively, a study by Jin et al. (2007) quantified NCP by combining an ecosystem model with an ocean circulation model to estimate global NCP at 14.9 ± 2.5 Pg C yr^{-1} .

1.2.2 Relationship of NCP to Air-Sea Flux

Air-sea flux is a function of the partial pressure of CO_2 ($p\text{CO}_2$) disequilibrium between the atmosphere and the ocean caused by physical and biological factors. It is affected by physical conditions that alter the solubility of CO_2 like sea surface temperature and salinity. Net community productivity is closely related to the process of air-sea flux because it is the biological driver of $p\text{CO}_2$. When production exceeds respiration, the ecosystem shifts towards autotrophy and the surface ocean becomes under-saturated in CO_2 causing an air-to-sea flux of CO_2 . Conversely, the ecosystem will become heterotrophic if respiration outpaces production. Then the surface ocean super-saturates with CO_2 and a sea-to-air flux will occur. Despite the importance of NCP to surface CO_2 fluxes, little work has been done to deconvolve NCP in coastal systems. Prowe et al. (2009) specifically addressed the mechanisms driving air-sea flux in the North Sea and found that in the northern region, air-sea flux

was more biologically driven, but in the southern region, temperature was a more influential driver than the biology. In the marsh-dominated South Atlantic Bight, net metabolism was found to be $0.004 \text{ Pg C yr}^{-1}$ (Cai et al., 2003) while coral reef metabolism in Moorea, French Polynesia was found to decrease total seawater CO_2 by $5.2 \times 10^{-15} \text{ Pg m}^{-2} \text{ d}^{-1}$ (Gattuso et al., 1993). Another study of 27 estuaries showed all but four to be heterotrophic (Caffrey, 2003), and a study of the Scheldt estuarine plume found it to be heterotrophic for three years but autotrophic one year, likely due to increased nutrient input from freshwater discharge (Borges et al., 2008).

Significantly more work has been focused on elucidating coastal air-sea fluxes of CO_2 . These can be estimated from pCO_2 and wind speed, which is used to parameterize gas transfer velocity (Liss and Merlivat, 1986; Wanninkhof, 1992; Wanninkhof and McGillis, 1999; Nightingale et al., 2000). A heated debate has ensued over the status of the coastal ocean in the global carbon cycle. A study of nine European estuaries were found to emit $0.03\text{-}0.06 \text{ Pg C yr}^{-1}$ to the atmosphere (Frankignoulle et al., 1998), while a study in the South Atlantic Bight also showed a sea-to-air flux of $0.0027 \text{ Pg C yr}^{-1}$ (Cai et al., 2003). Only one study has been done in the GoM, which found it to be a source of $4.56 \times 10^{-15} \pm 3.12 \times 10^{-15} \text{ mol C m}^{-2} \text{ yr}^{-1}$ to the atmosphere (Vandemark et al., 2011). On the other hand, Borges and Frankignoulle (2002) found the Galician Coast of Spain to be a net sink, and Kortzinger (2003) found the total net air-sea flux associated with the Amazon River plume in the Atlantic to be $0.014 \pm 0.005 \text{ Pg C yr}^{-1}$.

Clearly, a single generalization of the role of coastal regions cannot be made. More recently, it has been postulated that coastal regions differ according to latitude. Air-sea CO_2 fluxes were examined by Borges et al. (2005) based on an exhaustive literature survey. They found coastal regions at high and temperate latitudes to be sinks while subtropical and tropical latitudes were sources of CO_2 . These findings were corroborated by Cai et al. (2006), who compiled a database of continental shelf

air-sea fluxes and found shelf regions to be a sink of $0.33 \text{ Pg C yr}^{-1}$ in the middle and high latitudes and a source of $0.11 \text{ Pg C yr}^{-1}$ at low latitudes. Clearly, uncertainty still exists as to the status of the coastal ocean in the global carbon cycle. Thus, it is important not only to quantify air-sea flux but to understand the processes that influence it such as net community productivity.

1.2.3 Causes of Variability in Coastal NCP

The primary factors that influence NCP are the balance between inorganic nutrients and organic carbon in the system and the availability of light (Hopkinson and Vallino, 1995). Inorganic nutrient loading stimulates production leading to autotrophic conditions, whereas labile organic carbon loading fuels heterotrophy. Factors that influence the photosynthetic process also impact NCP such as solar irradiance and turbidity, which reduces the amount of light that phytoplankton receive, as well as inputs of nutrients from upwelling and vertical mixing. It has also been demonstrated that seasonal shifts towards autotrophy can occur during the spring phytoplankton bloom even though the system is net heterotrophic the rest of the year (Caffrey et al., 1998).

Additionally, several studies have shown water mass properties to be correlated to metabolism in estuaries. In a study of 27 estuaries monitored by the National Estuarine Research Reserve (NERR), Caffrey (2003) found a strong correlation between temperature and metabolic rate, with warmer temperatures leading to higher metabolic rates and consequently more heterotrophic conditions. The same study also observed a correlation between salinity and metabolic rates; however, this connection was less clear. Some locations had more autotrophic conditions at high salinities while some had more heterotrophic conditions at high salinities. Caffrey (2003) attributed this to differing freshwater inputs at each site, where more autotrophic conditions indicated nutrient-rich runoff and increased heterotrophic conditions suggested highly

organic runoff. A follow-up study of 42 sites within the NERR was conducted to assess how metabolic rates were affected by physical, chemical, and biological variables (Caffrey, 2004). It was found that temperature, followed by nutrients, were the two most important factors in explaining intra-site variation of metabolic rates, while adjacent habitat, estuarine area, and salinity were able to explain 58% of the variation between sites (Caffrey, 2004).

1.2.4 Optical Parameters for Estimation of NCP

Although considerable prior work has been done to calculate net primary production (Antoine et al., 1996; Behrenfeld and Falkowski, 1997) from satellite ocean color data, little if any work has focused on estimating NCP. We hypothesize that NCP is related to changes in particle stocks, which have been shown to be empirically related to optical data, in particular particle attenuation and particle backscattering. Additionally, we will look at chlorophyll-*a* (chl-*a*) and use an appropriate C:Chl ratio to convert chl-*a* to carbon. We believe one or more optical parameters may serve as a good indirect proxy for NCP, in which case NCP could be tracked remotely by satellite.

Satellite optical remote-sensing strives to understand how light interacts with seawater and its constituents to estimate optical properties. Most light penetration occurs in the visible range (400-700 nm). When light penetrates the water, it can either be absorbed or scattered. These terms are quantified by the absorption coefficient (*a*) and the scattering coefficient (*b*) at various wavelengths (λ). The sum of these two is the attenuation coefficient (*c*). They are considered inherent optical properties (IOPs) of seawater because they are only dependent on the constituents of the water (Kirk, 1994).

Absorption

Absorption converts light into heat or chemical energy (biomass from photosynthesis). Light absorption in the ocean is due to four components: seawater, phytoplankton, non-algal particles such as minerals and detritus, and colored dissolved organic matter (CDOM), which comes from compounds called humic substances in soil that drain into the ocean from rivers. The total absorption coefficient, a , is the summation of the absorption coefficients of each component respectively

$$a(\lambda) = a_w(\lambda) + a_{ph}(\lambda) + a_p(\lambda) + a_{CDOM}(\lambda) \quad (1.2)$$

Seawater absorption is strongest in the red (680 nm) and weakest in the blue-green. Phytoplankton, on the other hand, absorb predominantly blue light due to the photosynthetic pigment chl-*a*. Chlorophyll-*a* also absorbs in the red, while yellow accessory pigments called carotenoids absorb in the green. In the presence of high irradiance, chl-*a* will re-emit photons at lower energy. This phenomenon is known as fluorescence. Generally, higher chlorophyll concentrations result in more fluorescence, thus, fluorescence can be used as an index of chl-*a* concentration.

Much work has been done to isolate a_{ph} . Phytoplankton communities vary largely in shape, size, and pigment composition, which can cause differences in absorption (Ciotti et al., 2002). Pigment packaging is thought to be related to cell size and can further influence absorption. Ciotti et al. (2002) compared absorption spectra for phytoplankton communities of different sizes and found that more than 80% of the variability in the spectral shape of a_{ph} was determined by the cell size of the most abundant organism. According to Ciotti et al. (2002), the influence of cell size is actually a proxy for several changes at once because of the covariation of pigment packing and the concentration of accessory pigments with cell size. Variation in a_{ph} as a result of pigment packing related to cell size was further supported by Bricaud et al. (2004).

Scattering

Scattering occurs when light interacts with a substance in the water that causes it to change direction (Kirk, 1994). Scattering can occur in both the forward and backward directions. The total scattering coefficient is the summation of the two

$$b(\lambda) = b_f(\lambda) + b_b(\lambda) \quad (1.3)$$

where b_f is the forward scattering coefficient and b_b is the backscattering coefficient. Backscattering can be further partitioned into backscattering by seawater and by particles

$$b_b(\lambda) = b_{bw}(\lambda) + b_{bp}(\lambda) \quad (1.4)$$

where b_{bw} is the backscattering coefficient of pure seawater and b_{bp} is the backscattering coefficient of particles. The scattering of light by seawater is caused by changes in the density of water molecules due to temperature, salinity, and pressure (Stramski et al., 2004). Particles that cause scattering include mineral particles, phytoplankton, bacteria, and dead cells (Kirk, 1994). The size, shape, and structure of these various particles affects how much light will be scattered (Stramski et al., 2004). Coastal waters tend to have more scattering than the open ocean due to phytoplankton, terrigenous material from rivers, and resuspended sediments from wave action, storms, and tidal currents (Kirk, 1994).

Stramski et al. (1999) were the first to show that POC could be estimated by satellite-derived particle backscattering. Their work centered on two empirical relationships. The first relationship derived b_b from satellite remote-sensing reflectance, which can be used to calculate b_{bp} . The second relationship connected b_{bp} to surface POC. However, Stramski et al. (1999) showed that the b_{bp} to POC relationship differed regionally between two locations in the Southern Ocean, suggesting the need for site-specific algorithms. Further work has been done to develop b_{bp} to POC algorithms in the Mediterranean Sea (Loisel et al., 2001) and improve the algorithms for the Southern Ocean (Allison et al., 2010).

Attenuation

When the scattering coefficient is added to the absorbance coefficient, the result is the attenuation coefficient (c)

$$c(\lambda) = a(\lambda) + b(\lambda) \quad (1.5)$$

The beam attenuation coefficient can be decomposed into the attenuation of its constituents

$$c(\lambda) = c_w(\lambda) + c_{\text{CDOM}}(\lambda) + c_p(\lambda) \quad (1.6)$$

where c_w , c_{CDOM} , and c_p are the attenuation coefficients of seawater, CDOM, and particles respectively. A wavelength of 660 nm is generally used because $c_{\text{CDOM}}(660)$ is insignificant in oligotrophic waters (Bricaud et al., 1981). The beam attenuation of seawater is constant so its effects can be removed to calculate c_p .

Bishop (1999) reviewed the literature attempting to correlate beam attenuation to particle volume and suspended mass concentration. He subsequently demonstrated that a better correlation independent of geographic region, season, and depth exists between beam attenuation and POC when measured by a multiple-unit large-volume in situ filtration system (MULVFS). Beam attenuation versus POC regressions yielded r^2 values of 0.97 and 0.95 for two cruises in the equatorial Pacific; however, regressions with bottle POC for the same two cruises returned r^2 values of 0.40. It is not clear why bottle POC and MULVFS-determined POC relationships are so different but Bishop (1999) suggests a re-evaluation of bottle POC methods. These results were supported within several percent by a similar experiment near southern Vancouver Island (Bishop et al., 1999).

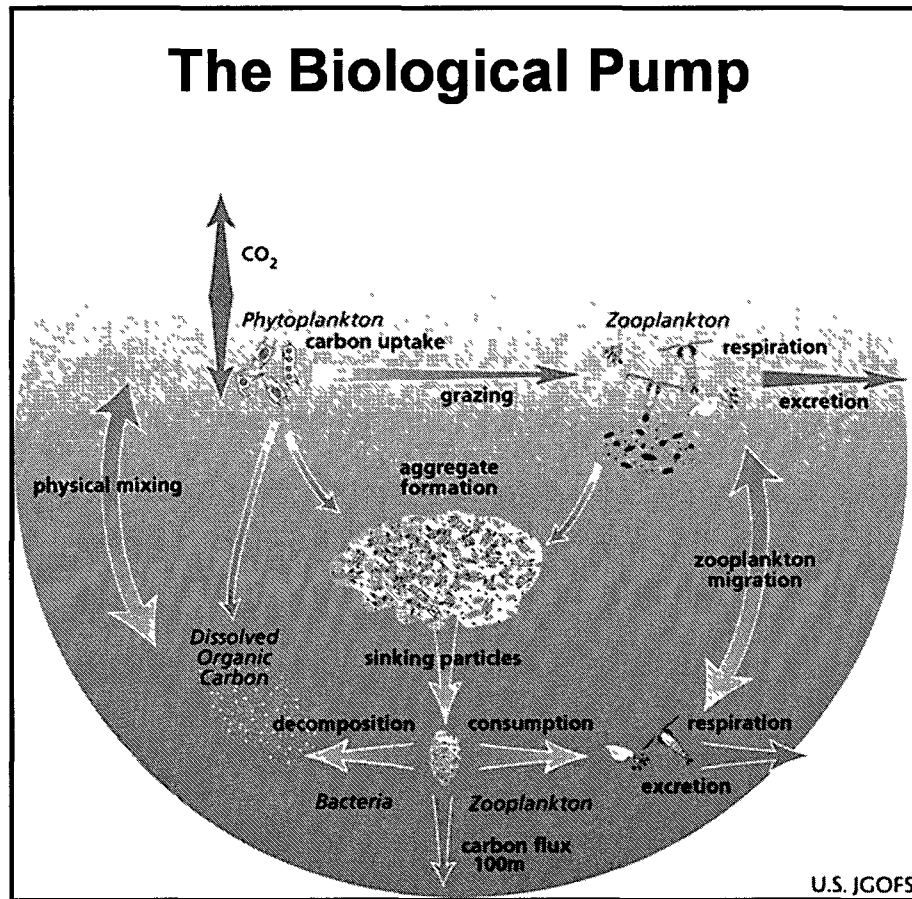


Figure 1-1: The ocean acts as a sink for CO_2 through a process known as the biological pump. Phytoplankton remove CO_2 from the surface waters and convert it to organic carbon during photosynthesis. A fraction aggregate and sink through the water column, while others are consumed by zooplankton who emit fecal pellets that sink. Through this sinking process, carbon is removed from the surface and exported to the deep ocean.

CHAPTER 2

DRIFTER STUDY

The first goal of this experiment was to characterize net community productivity in the western Gulf of Maine. This was accomplished by a cruise in which a water parcel was visited every other day over the course of two weeks and the time difference of vertical oxygen profiles was analyzed to calculate NCP. To that end, a proxy obtainable by satellite was sought. Optical proxies have successfully been used in the past, most notably chl-*a* as an index of phytoplankton biomass. If changes in phytoplankton stock are due to production and respiration, then it seems reasonable to assume that a change over time in chl-*a* would act as a proxy for NCP. Similarly, if c_p and b_{bp} can be used to estimate POC, and changes in POC are attributable to community productivity, then changes in c_p and b_{bp} should also be useful to indirectly measure NCP. The second goal of this experiment then was to evaluate chl-*a*, c_p and b_{bp} as potential indices for NCP.

2.1 Site Description

The Gulf of Maine is a highly productive continental-shelf sea extending from Cape Cod to Nova Scotia. It is separated from the Northwest Atlantic by Georges Bank and Browns Bank, with the Northeast Channel situated between these two banks serving as the primary conduit for exchange between the GoM and the open ocean. The GoM undergoes tidal mixing from semi-diurnal tides ranging from 2-3 m in the western Gulf to over 10 m in the Bay of Fundy (Townsend et al., 1987) that continuously deliver nutrients to the euphotic zone (Townsend et al., 2006). The western GoM is

also influenced by freshwater discharge from the area's major rivers including the St. John, the Merrimack, the Penobscot, and the Kennebec-Androscoggin system.

The major biological event of the year is the spring phytoplankton bloom. High biological productivity in the GoM has been linked to three processes working in concert to deliver nutrients into the GoM, mix them to the surface, and re-distribute them throughout the GoM. The delivery of nutrients occurs when deep slope water enters the GoM through the Northeast Channel (Townsend, 1998). The slope water can either be cold, fresh Labrador Slope Water (LSW) with nitrate concentrations of about 15 μM , or warmer and more saline Warm Slope Water (WSW) originating from the Gulf Stream with higher nitrate concentrations of $>23 \mu\text{M}$. Both LSW and WSW have silicate concentrations in the range of 10-14 μM (Townsend et al., 2006). The nutrient-rich water is then brought to the surface by tidal mixing and upwelling, vertical flux across the seasonal pycnocline, or winter convection (Townsend, 1991). During the summer, these processes can increase surface nitrate levels to $>7 \mu\text{M}$ (Townsend et al., 1987). Once at the surface, nutrients are distributed to the western GoM by the Eastern Maine Coastal Current (EMCC), which originates on the Nova Scotian Shelf and travels southwest, hugging Maine's coast, until it turns offshore near Penobscot Bay. The EMCC is essential for biological productivity in the GoM, transporting as much as 44% of the inorganic nutrients derived from slope water to the western GoM (Townsend et al., 1987).

2.2 Methods

2.2.1 Sample Collection and Analysis

Cruises aboard the University of New Hampshire's (UNH) R/V Gulf Challenger took place in the western Gulf of Maine on seven days between June 16, 2010 and July 2, 2010. In order to track a water parcel over the course of the cruises, a surface

drifter and a 12-meter drogue both outfitted with GPS units were deployed at roughly 43.7°N and -70.0°W. The drogue was placed at 12 m as that was the expected depth of the chlorophyll maximum. The surface drifter spiraled away to the east as the surface layer sheared off and we were unable to follow it. We tracked the 12-m drogue for the duration of the cruises and visited it approximately every other day where we stayed on station for 8-10 hours to collect samples, perform oxygen incubations, and take vertical profiles.

Discrete samples of dissolved oxygen, chl-*a*, and particulate organic carbon (POC) were taken at 2 and 12 meters with Niskin bottles to correct profiler data during data processing. Dissolved oxygen samples were collected in 300 mL borosilicate glass bottles, preserved with 1 mL of MnSO₄ solution and 1 mL of NaOH/KI solution, and analyzed by Winkler titration. Chlorophyll-*a* and POC samples were filtered through 25 mm Whatman GF/F glass fiber filters, wrapped in foil, and stored in liquid nitrogen. Chlorophyll-*a* was extracted from the filters with 7 mL of 90% acetone and analyzed by fluorometry (Turner Designs Aquafluor). The POC filters were saturated with HCl fumes, dried, and analyzed on a PerkinElmer 2400 Series II CHNS/O Elemental Analyzer. All analysis followed accepted JGOFS protocols (Knap et al., 1996).

Oxygen incubations were done in light and dark 300 mL borosilicate glass bottles. The light bottles were incubated in direct sunlight on deck, and the dark bottles were incubated in a covered chamber. Both light and dark bottles were maintained at sea-surface temperature by pumping surface water through the chambers. At the end of the incubations, the DO samples were preserved as described above and analyzed by Winkler titration.

Several vertical profiles were taken throughout the day with two profilers. The SBE profiler measured conductivity, temperature, and depth (Sea-Bird SBE 49), dissolved oxygen (Sea-Bird SBE 43), chlorophyll fluorescence (WET Labs ECO Fluor-

rometer), and photosynthetically active radiation (Biospherical QSP). The IOP profiler also measured absorption and attenuation (WET Labs ac-s) and backscattering (WET Labs ECO BB9) in addition to conductivity, temperature, depth (Sea-Bird SBE 49), dissolved oxygen (Sea-Bird SBE 43), and chlorophyll fluorescence (WET Labs ECO Fluorometer).

On the last day of the cruise, water samples were collected to determine the phytoplankton species present. Following Utermöhl's method, 200 mL samples were collected at depths of 2 m, 14 m, and 20 m. They were preserved with Lugol's solution to kill, stain, and weight the phytoplankton. The samples were allowed to settle for 24 hours, and then the phytoplankton were identified and counted with an inverted microscope.

2.2.2 Data Processing

Profiler Corrections

Raw oxygen data from the vertical profiles needed to be corrected due to calibration drift in the instruments. Oxygen data from the two profilers were plotted against discrete oxygen samples in order to apply an offset to the data from the instruments. A linear regression was fitted to the data, and the slope and intercept were used to correct the oxygen profiles (Fig. 2-1). Similarly, the f-chl data were plotted against discrete chl-*a* samples and fitted with a linear regression (Fig. 2-2). The slope and intercept were used to convert f-chl to chl-*a*.

Biological Oxygen Anomaly

Variability in dissolved oxygen is attributable to biological and physical factors. Biological additions of oxygen to seawater are the result of photosynthesis while consumption of oxygen occurs during respiration. The physical factors that affect dissolved oxygen are temperature, salinity, and pressure, which alter the solubility of

oxygen in seawater. In order to calculate NCP from oxygen data, the changes in oxygen due solely to biology must be isolated. We will call this the biological oxygen anomaly ($\Delta[O_2]_{bio}$). The expected oxygen at saturation was calculated as a function of temperature and salinity according to Weiss (1970). The change in oxygen due to biological production was then calculated as

$$\Delta[O_2]_{bio} = [O_2] - [O_2]_{sat} \quad (2.1)$$

so as to remove the effects of solubility. $[O_2]$ is the corrected oxygen concentration and $[O_2]_{sat}$ is the expected oxygen concentration at saturation.

Net Community Production from Oxygen

Net community productivity derived from oxygen (NCP_{O_2}), was calculated by integrating the biological oxygen anomaly from 1 m to the average euphotic depth (z_{eu}) of 24 m to get an oxygen inventory. Oxygen was integrated from 1 m because the first meter of data was unreliable. The euphotic depth was calculated from the photosynthetically active radiation (PAR) sensor on the profiler for each cast. The average euphotic depth was chosen for the integration depth because PAR may have varied significantly if the sun went behind the clouds during a particular cast, but this likely would not have affected the water column distribution over such short time scales. The change in oxygen stock was calculated and then corrected for the loss or addition of oxygen at the surface due to air-sea flux and bubble injection, and the loss of oxygen at the euphotic depth due to diffusion:

$$NCP_{O_2} = \frac{\partial}{\partial t} \left(\underbrace{\int_1^{z_{eu}} \Delta[O_2]_{bio} \partial z}_{\Delta O_2 \text{ Stock}} + \underbrace{\int_{t_1}^{t_2} F_s \partial t}_{\text{Air-Sea Flux}} - \underbrace{\int_{t_1}^{t_2} F_i \partial t}_{\text{Bubble Injection}} + \underbrace{\int_{t_1}^{t_2} F_d \partial t}_{\text{Diffusion}} \right) \quad (2.2)$$

Air-sea flux (F_s), bubble injection (F_i), and diffusion (F_d) were all integrated from an initial cast (t_1) to a subsequent cast (t_2). NCP was considered over two timescales: over the course of the day (last cast minus first cast) and between casts. Advection

was considered negligible since we were tracking a water parcel. The final NCP_{O_2} was converted to units of carbon using the Redfield ratio.

Air-Sea Flux and Bubble Injection

Air-sea gas exchange occurs when the partial pressures of gases in the ocean are not at equilibrium with atmospheric concentrations. Gas interactions at the atmosphere-ocean interface can then represent an addition or loss of CO_2 and O_2 to the system that is independent of biological consumption and production of these gases. As a result, gas exchange must be accounted for in our NCP measurements. Air-sea gas exchange and bubble injection are functions of wind speed, which causes turbulent waves that increase the surface area for gas exchange (Libes, 1992). Bubble injection was determined according to Nicholson et al. (In Press). Air-sea flux (F_s) for O_2 was estimated from:

$$F_s = k(C_{sw} - C_{sat}) \quad (2.3)$$

where C_{sw} is the measured O_2 concentration and C_{sat} is the expected O_2 concentration at saturation. The rate at which a column of gas will diffuse through the water column, known as the piston velocity, can be estimated from wind speed (Liss and Merlivat, 1986; Wanninkhof, 1992; Wanninkhof and McGillis, 1999; Nightingale et al., 2000). Piston velocity (k) was computed according to Nightingale et al. (2000)

$$k = (0.333 u_{10} + 0.2222 u_{10}^2) \left(\frac{Sc}{600} \right)^{-0.5} \quad (2.4)$$

Wind speed (u) at 4 m was obtained from the Gulf of Maine Ocean Observing System's (GoMOOS) Buoy B and converted to windspeed at 10 m (u_{10}) after Smith (1988). The Schmidt number (Sc) was calculated as

$$Sc = \frac{\text{kinematic viscosity}}{\text{diffusivity}} \quad (2.5)$$

Diffusivity was determined according to the Arrhenius equation with the activation energy and pre-exponential factor taken from Emerson and Hedges (2008). Kinematic

viscosity is the ratio of dynamic viscosity to density. Density was computed after Fofonoff and Millard (1983) and dynamic viscosity was estimated from Sharqawy et al. (2010).

Diffusion

Diffusion of oxygen occurs at the base layer of the euphotic zone where oxygen concentrations are higher in the euphotic zone than below. The diffusive flux (F_d) was calculated by

$$F_d = k_z \frac{\partial [O_2]}{\partial z} \quad (2.6)$$

where 5 m (2.5 m above and below the euphotic depth) was chosen as ∂z . A diffusivity constant (k_z) of $1.5 \text{ cm}^2 \text{ s}^{-1}$ found for stratified July conditions in the Wilkinson Basin section of the Gulf of Maine was taken from Benitez-Nelson et al. (2000).

Net Community Productivity from Optical Parameters

In order to compare NCP_{O_2} to our optical parameters (chl-*a*, c_p , and b_{bp}), they were first converted to carbon. It was determined that we were tracking an *Alexandrium* bloom on the cruise so chl-*a* was converted to units of carbon by applying a C:Chl ratio of 172, found by Langdon (1987) for *Gonyaulax tamarensis* (*Alexandrium tamarense*) at high irradiance. $c_p(660)$ and $b_{bp}(555)$ were linearly regressed against discrete POC samples to derive empirical relationships (Fig. 2-3). The slope and intercept were applied to convert $c_p(660)$ and $b_{bp}(555)$ to POC.

Net community production of organic carbon (NCP_{OC}) for each parameter was subsequently estimated as

$$\text{NCP}_{OC} = \frac{\partial}{\partial t} \left(\underbrace{\int_1^{z_{eu}} \Delta POC \partial z}_{\Delta \text{Particle Stock}} + \underbrace{\int_1^{z_{eu}} \Delta DOC \partial z}_{\text{Extracellular Production}} + \underbrace{\int_{t_1}^{t_2} F_g \partial t}_{\text{Gravitational Flux}} \right) \quad (2.7)$$

As with oxygen, POC was integrated from 1 m to the average euphotic depth. However, POC production by phytoplankton only represents a fraction of the change in carbon stock due to biology, so dissolved organic carbon (DOC) produced by phytoplankton (extracellular release) must also be taken into account. Little is known about extracellular release but it is thought to be the result of one of two physiological mechanisms: (1) an overflow mechanism to release excess photosynthate (Fogg, 1983) or (2) passive diffusion of photosynthates (Bjørnsen, 1988). The percent of extracellular release (PER) is defined as

$$\text{PER} = \frac{\text{DOC}_p}{\text{DOC}_p + \text{POC}_p} \quad (2.8)$$

where DOC_p and POC_p are the photosynthetic production of DOC and POC respectively. Experiments by Marañón et al. (2004) found that PER was independent of phytoplankton biomass and productivity and that 80% of variability in integrated DOC_p was explained by POC_p , thus supporting the passive diffusion mechanism. The research by Marañón et al. (2004) suggested that productivity is underestimated if dissolved components are not accounted for. Therefore, we estimated DOC_p based on our POC_p and an average PER of 19% obtained by Marañón et al. (2004).

The vertical sinking, or gravitational carbon flux of POC must also be considered. Packard and Christensen (2004) explored vertical carbon flux in the Gulf of Maine at 30, 50, and 100 m depth by integrating respiratory oxygen consumption profiles. Given that 30 m was close to our average euphotic depth of 24 m, we applied a constant carbon flux of $3.09 \mu\text{mol m}^{-2} \text{min}^{-1}$ measured by Packard and Christensen (2004).

2.3 Results

2.3.1 Hydrography

The conditions over the course of the cruises were relatively stable. Surface temperatures began around 15 °C during the first week of sampling, and peaked at 22 °C after the end of the first week (Fig. 2-4). The temperatures then cooled back down to about 15 °C by the end of the second week of cruises. At 10 m depth, temperatures dropped by several degrees, and below 15 m, temperatures remained uniform around 8 °C. Salinity was uniform over time and increased by about 1.5 psu over 40 meters (Fig. 2-5). Fluorescent chlorophyll data exhibited surface chlorophyll values near 1 mg m⁻³ and a deep chlorophyll maximum (DCM), which occurred at 12 m on the first day of the cruise, and slowly deepened throughout the two week period. The DCM also increased in intensity, with the highest values at the end of the first week on June 25. The biological oxygen anomaly followed suite, with maximum values near 10 m at the beginning of the cruise, which deepened and increased in intensity over the course of the cruises. As expected, values were generally positive above the average euphotic depth (24 m), indicative that photosynthesis was the dominant process, whereas respiration prevailed below the euphotic depth.

2.3.2 Oxygen Corrections

Air-sea fluxes were calculated from piston velocity, which was parameterized from wind speed and the Schmidt number. Surface oxygen Schmidt numbers exhibited a decreasing trend over the course of the cruises (Fig. 2-8). Initial values were around 600 and declined to about 545 by the last cruise day. Ten-meter wind speeds were relatively low throughout the duration of the cruises with the average wind speed less than 5 m s⁻¹ (Fig. 2-9). The highest wind speeds of between 8 and 11 m s⁻¹ occurred on the third cruise day. Piston velocity mirrored wind speed with the highest values

between 17 and 35 cm hr^{-1} occurring on the third day during strong winds (Fig. 2-10). Mean piston velocity was 8.46 cm hr^{-1} .

Final air-sea fluxes ranged from 0.17 to 3.47 $\text{mmol m}^{-2} \text{hr}^{-1}$ out of the ocean. The mean air-sea flux over the course of the day was 1.52 $\text{mmol m}^{-2} \text{hr}^{-1}$ and 1.48 $\text{mmol m}^{-2} \text{hr}^{-1}$ between casts. The lowest overall fluxes occurred on the first cruise day, while the highest fluxes occurred on the June 30 cruise. As a percent of the change in oxygen stock, air-sea flux was the biggest correction. The mean percent of the change in oxygen stock, excluding two extremely high percentages ($>100\%$), was 14% over the day and 6% between casts. The high percentages were not the result of air-sea flux being high, but instead were due to very small changes in the oxygen stock.

Bubble injection was calculated as a function of wind speed, temperature, and salinity. At 10-meter wind speeds (u_{10}) less than 2.27 m s^{-1} , bubble injection was assumed zero. Fluxes due to bubble injection ranged from 0-1.14 $\text{mmol m}^{-2} \text{hr}^{-1}$ (Fig. 2-12). The mean rate of bubble injection was 0.14 $\text{mmol m}^{-2} \text{hr}^{-1}$ over the day and 0.13 $\text{mmol m}^{-2} \text{hr}^{-1}$ between casts. The highest bubble injection rates occurred on the third cruise day when the winds were strongest, while the bubble injection rates were below 0.40 $\text{mmol m}^{-2} \text{hr}^{-1}$ for the rest of the cruise days. Mean bubble injection flux was about 2% of the change in oxygen stock over the day and less than 1% between casts.

Diffusion of oxygen generally occurred from the base of the euphotic zone to the depths below. Positive diffusion values ranged from 0.12 $\text{mmol m}^{-2} \text{hr}^{-1}$ to 2.36 $\text{mmol m}^{-2} \text{hr}^{-1}$ (Fig. 2-13). Average values were around 0.89 $\text{mmol m}^{-2} \text{hr}^{-1}$ over the day and 0.87 $\text{mmol m}^{-2} \text{hr}^{-1}$ between casts. In a few cases, diffusion values were negative implying a movement of oxygen into the euphotic zone from below. These values ranged from 0.08 to 0.50 $\text{mmol m}^{-2} \text{hr}^{-1}$. As a percent of the change in oxygen stock, diffusion was an average of 9% over the day and 5% between casts

when excluding one unusually high value of over 100%. The high percentage was not a function of the diffusion value but of the oxygen change, which was unusually small.

2.3.3 Net Community Productivity

Final net community productivities were calculated after correcting the change in depth-integrated oxygen for air-sea flux, bubble injection, and diffusion (Fig. 2-14). Some variability in NCP occurred during the cruises. NCP values ranged from -2.64 to 2.11 g C m⁻² hr⁻¹. The mean rate of productivity was -0.04 g C m⁻² hr⁻¹ over the day and -0.07 g C m⁻² hr⁻¹ between casts. This indicates that the GoM was nearly in equilibrium during our cruises in spite of the variability that occurred. The last day of the cruise appeared to be the most productive with the majority of NCP being positive.

2.3.4 Optical Proxies for NCP

Linear regression analysis of NCP_{OC} derived from chl-*a*, $c_p(660)$, and $b_{bp}(555)$ showed promise as optical proxies for NCP_{O₂}. Because the coefficients of determination for the conversion of f-chl to chl-*a* and the conversion of $c_p(660)$ and $b_{bp}(555)$ to POC were not optimal (all <0.50), direct relationships between the change in f-chl, $c_p(660)$, and $b_{bp}(555)$ with NCP_{O₂} were also examined. Relationships were assessed over two time scales: NCP over the course of the day (last cast minus the first cast) and short-term NCP between each cast. P-values less than 0.05 were considered significant.

The relationship of NCP_{OC} derived from chl-*a* (NCP_{OC}(chl-*a*)) versus NCP_{O₂} over the course of the day (Fig. 2-15) was insignificant ($p = 0.12$, $r^2 = 0.18$). Short-term changes between casts (Fig. 2-16) were significant and showed a stronger correlation ($p < 0.001$, $r^2 = 0.40$). However, given that the same value is being measured on both axes, a 1:1 relationship was expected, yet the slope (m) is only 0.14. The

lack of a 1:1 relationship may be the result of the poor conversion of f-chl to chl-*a*. Surprisingly, when $NCP_{OC}(f\text{-chl})$ is regressed against NCP_{O_2} over the course of the day and between casts (Figs. 2-17 and 2-18), the results worsen ($p = 0.29$, $r^2 = 0.09$ and $p < 0.001$, $r^2 = 0.35$ respectively). While f-chl is not the equivalent of chl-*a*, NCP is a measure of the rate of change over time so it was expected that the change in f-chl should approximate the change in chl-*a* and the results would improve since no error was introduced by converting f-chl, however, this was not the case.

The strongest trends were found between NCP_{OC} derived from c_p ($NCP_{OC}(c_p)$) both throughout the day (Fig. 2-19) and between casts (Fig. 2-20). Both relationships were significant and strongly correlated ($p < 0.01$, $r^2 = 0.86$ and $p < 0.001$, $r^2 = 0.91$ respectively). Similarly, a 1:1 relationship was expected from $NCP_{OC}(c_p)$, however, the slope was only 0.18 during the day and improved to 0.28 between casts. Interestingly, when the change in depth-integrated $c_p(660)$ was regressed against NCP_{O_2} (Fig. 2-22) between casts, a 1:1 agreement was obtained ($m = 0.99$, $p < 0.001$), although the relationship weakens slightly ($r^2 = 0.88$). However, this 1:1 relationship was not seen throughout the day (Fig. 2-21) where the slope was only 0.48 ($p < 0.05$).

The trend between NCP_{OC} derived from b_{bp} ($NCP_{OC}(b_{bp})$) and NCP_{O_2} was insignificant over the course of the day ($p > 0.05$) despite an r^2 of 0.54 (Fig. 2-23). A significant correlation was found between casts ($p < 0.001$, $r^2 = 0.83$), although a 1:1 relationship was still not seen (Fig. 2-24). Plotting $b_{bp}(555)$ with NCP_{O_2} did not improve the slope as backscattering is a very small portion of the attenuation in an ecosystem dominated by productivity (Antoine et al., 2011).

2.4 Discussion

This experiment sought to characterize NCP in the western GoM and analyze the potential of several optical variables as proxies for NCP that would offer the opportunity to estimate NCP globally and improve oceanic carbon budgets. At the start of this work, there were three main points of contention: 1) a suitable depth of integration to calculate inventories, 2) the implications of surface shear to tracking a water mass, and 3) an appropriate C:Chl ratio for conversion of chl-*a* into units of carbon.

At first glance, the mixed layer depth (MLD) seemed to be the relevant depth of integration. However, when MLDs were calculated based on potential density and temperature using thresholds of 0.03 and 0.2 respectively after de Boyer Montégut et al. (2004), MLDs were found to be on average 5 meters. Upon examination of the biological oxygen and f-chl profiles, maxima were well below the MLD suggesting that most of the biological activity would be ignored when only integrating to the MLD. Consequently, the euphotic depth, or the depth to which 1% of surface light penetrates, was chosen as the integration depth to ensure that the most biological activity would be captured.

As for the second issue, originally this experiment was intended to be a Lagrangian cruise that would track one water mass over the course of two weeks. At the outset of this experiment, a surface drifter and 12-m drogue were deployed, but the surface layer of water sheared off and carried the surface drifter to the east while we tracked the drogue south. Kudryavtsev and Soloviev (1990) describes this phenomenon in the Equatorial Atlantic as the result of daytime solar heating causing a decreased drag coefficient in the near-surface layer allowing it to slip over the underlying water with little friction. Wind stress can then induce a current in the surface water that moves it in another direction than the water below. This has repercussions for our experiment because the surface water above the thermocline was moving away

so our cruise was not truly Lagrangian. While we were tracking the 12-m water mass, we had different surface water during each sampling period. However, since the surface layer was shallow (<5 m) and most of the biological activity occurred below 12 meters, this likely introduced little error to our NCP calculations.

With regard to the third point, a first approximation of the C:Chl ratio was made using a ratio of discrete POC data to discrete chl-*a* data resulting in a ratio of 230. However, the ratio of POC to chl-*a* is an overestimation of the C:Chl ratio because POC includes both living and detrital components. Since we were unable to isolate the living component of POC, we used the ratio of 172 found by Langdon (1987) at high light conditions, which seemed an appropriate value more representative of the living component of POC. As we were unable to calculate our own C:Chl ratio, significant error may be associated with using a value from the literature, although it seems a reasonable estimate. Similar values of 172, 180, and 82 were found by Buck et al. (1996) for the tropical, subtropical, and subarctic regions of the North Atlantic respectively.

2.4.1 Sources of Error

Estimating the uncertainty in NCP calculated from both oxygen and POC was a challenging task because errors propagated with each correction. In order to estimate the total uncertainty, a Monte Carlo analysis was utilized. This involved generating random samples for each variable that was subject to error within the NCP equation based on their mean and standard deviation. Some of these variables were measured directly while those that could not were taken from the literature. A summary of the means and uncertainties of each parameter used to calculate NCP_{OC} and NCP_{O_2} is given in Tables 2.1 and 2.2.

The lack of a 1:1 relationship between NCP_{O_2} and NCP calculated from optical proxies is indicative that either not enough particles were added back in or too much

oxygen was added when correcting for fluxes. This could arise from the ineffective tracking of particle loss or O_2 gain. According to the Monte Carlo analysis, the largest errors in the estimation of NCP_{O_2} came from air-sea flux, followed by diffusion. Since wind speeds were low, bubble injection was of least importance. The largest error incorporated into NCP_{OC} came from ΔDOC . In all NCP estimates, uncertainties were extremely high, particularly in $NCP_{OC}(c_p)$, which gave the best relationship with NCP_{O_2} .

The first source of error associated with NCP_{OC} involves the conversion of c_p and b_{bp} to POC. Literature reports strong linear relationships when regressing c_p and b_{bp} against POC with $r^2 > 0.80$ (Gardner et al., 1993; Bishop, 1999; Bishop et al., 1999; Stramski et al., 1999; Mishonov et al., 2003). But our relationships for c_p and b_{bp} against bottle POC were weak ($r^2 = 0.48$ and $r^2 = 0.37$ respectively). As mentioned previously, Bishop (1999) observed the same poor relationship with bottle POC data ($r^2 = 0.40$), but achieved an $r^2 > 0.90$ with *in situ* POC filtration methods. In spite of these weak relationships, NCP regressions were more robust with NCP calculated from POC than when plotted directly with c_p and b_{bp} .

Large errors in NCP_{OC} estimations were also associated with the conversion of chl-*a* to carbon, gravitational flux, and extracellular release because we were unable to directly measure these values. Instead values from the literature were assumed, which introduced more error than if we had been able to measure them directly. Although the largest error according to the Monte Carlo analysis came from ΔDOC , the vertical sinking flux may well be causing even greater error as this value was taken from the literature in a study done in 2004. It is unlikely that vertical sinking rates are constant over the years and sinking fluxes can change quickly during flash events where many particles may be lost. Thus, studies of gravitational fluxes are needed on shorter time scales.

Errors associated with NCP_{O_2} were related to piston velocity, air-sea flux, dif-

fusion, and bubble injection corrections. While errors were high, values compared relatively well to the literature values that were scaled down to hourly rates. Winds were fairly calm during the duration of our cruises, with average u_{10} of $\sim 4 \text{ m s}^{-1}$. The mean piston velocity was $2.4 \times 10^{-3} \text{ cm s}^{-1}$, which is in good agreement with the piston velocity of $4 \times 10^{-3} \text{ cm s}^{-1}$ found by Redfield (1948) in the summer for the GoM. It is also similar to the piston velocity of $4.1 \times 10^{-3} \text{ cm s}^{-1}$ in the shelf area west of Iceland where average wind speed was 4.4 m s^{-1} (Stefánsson et al., 1987) and the piston velocity of $1.6 \times 10^{-3} \text{ cm s}^{-1}$ found by Johnson and Pytkowicz (1979) in Stuart Channel, BC.

The average air-sea flux ($1.52 \text{ mmol m}^{-2} \text{ hr}^{-1}$) was a little higher than air-sea fluxes found by Álvarez et al. (2002) in Bellingshausen Sea (Antarctic waters). In Bellingshausen Sea, a diatom bloom occurred during the study period causing the area to act as a strong source of oxygen $1.04 \text{ mmol m}^{-2} \text{ hr}^{-1}$ similar to the *Alexandrium* bloom seen in our study. During two wind events ($5 < u_{10} < 11 \text{ m s}^{-1}$) in Martha's Vineyard, McNeil et al. (2006b) reported air-sea fluxes of 0.53 and $-1.81 \text{ mmol m}^{-2} \text{ hr}^{-1}$, which are similar in magnitude to our data.

Bubble flux was seldom reported in the literature, likely due to the uncertainty in modelling it. Najjar and Keeling (2000) employed the Spitzer and Jenkins (1989) model to calculate a global mean annual bubble injection flux of $2 \text{ mol m}^{-2} \text{ yr}^{-1}$. When scaled down to an hourly flux of $0.23 \text{ mmol m}^{-2} \text{ hr}^{-1}$ it correlates well to our mean bubble injection flux of $0.14 \text{ mmol m}^{-2} \text{ hr}^{-1}$. Good agreement was also found with an annual estimation by Hamme and Emerson (2006) of $0.16 \text{ mmol m}^{-2} \text{ hr}^{-1}$ when scaled down to an hourly flux at station ALOHA near Hawaii.

There is also a paucity of literature reporting diffusive flux of oxygen across the euphotic depth. McCardell and O'Donnell (2009) reported fluxes of $150\text{-}160 \text{ mmol m}^{-2} \text{ d}^{-1}$ across the pycnocline in the Long Island Sound, however, this is likely not a good comparison as they state that the euphotic depth is much shallower than

the pycnocline in Long Island Sound. Kemp and Boynton (1980) reported that in Chesapeake Bay, diffusive flux ranged from 1-9% of the total inputs and outputs across the euphotic boundary, with an average of 5%. Our diffusive flux corresponded well with an average of 9% of the total oxygen inputs and outputs.

2.4.2 Net Community Productivity

Despite large errors, our NCP rates correspond well to literature values. Sambrotto and Langdon (1994) conducted a Lagrangian experiment on Georges Bank during April of 1990 by following a water mass spiked with SF₆ for 10 days. NCP was calculated from changes in DIC and O₂ resulting in average NCP from -0.05 to -0.06 g C m⁻² hr⁻¹ using both methods, which compares well to our average NCP of -0.04 to -0.07 g C m⁻² hr⁻¹. Further studies in the Labrador Sea by Martz et al. (2009) became Lagrangian when a mooring became loose in late June-August of 2004. They estimated NCP of 0.02 g C m⁻² hr⁻¹, which is near equilibrium like our estimate.

Marra et al. (1995) did similar work in the northeast Atlantic following drifters over three periods in 1991. The first was during a bloom of *Paecocystis pouchetii*, the second occurred after a storm mixed the water column to a MLD of >150 m, and the third deployment was during the restratification of the water column. They also found a good correlation between c_p and chl-*a* to POC and subsequently estimated POC from both. Upon comparison of NCP from O₂ and POC, they were mildly successful in their comparison. During stations before the storm, they only observed agreement in sign while after the storm, values agree to 30%. As with our study, their NCP rates from POC estimated by c_p were off by a factor of 4.6 (similar to our nearly 5) when compared to NCP rates from O₂ measurements.

Lastly, Jönsson et al. (2010) did the only study we are aware of that attempts to estimate NCP with satellite ocean color data from MODIS-Aqua. The study in

the GoM over 3 years used chl-*a* and light attenuation in conjunction with a C:Chl model to calculate phytoplankton carbon inventories down to the euphotic depth. NCP was estimated from changes in phytoplankton carbon stocks using sequential satellite images that tracked water parcel movements. They were successful and found that NCP values ranged from $\pm 0.02 \text{ g C m}^{-2} \text{ hr}^{-1}$, similar to the values in our experiment.

2.4.3 Optical Proxy Relationships

$\text{NCP}_{\text{OC}}(c_p)$ showed the strongest relationship to NCP_{O_2} , both over the day and between casts. According to Behrenfeld and Boss (2003), c_p should be closely associated with phytoplankton carbon biomass since c_p is dominated by particles in the phytoplankton size domain (0.5-2.0 μm). While inorganic, detrital, and heterotrophic particles can also cause variability in c_p , it is assumed that variations in c_p were due solely to biology over short time scales of our study. Although c_p is not currently a remote sensing product, advances are being made to retrieve c_p from water leaving radiance (Roesler and Boss, 2003).

$\text{NCP}_{\text{OC}}(b_{\text{bp}})$ also showed relatively good trends, although they were not as strong as those from $c_p(660)$. This is probably due to the fact that most backscattering is caused by particles less than 1 μm (Stramski and Kiefer, 2001), the majority of which are thought to be detrital (non-living) particles (Ulloa et al., 1994). $\text{NCP}_{\text{OC}}(\text{chl-}a)$ displayed little to no correlation with NCP_{O_2} . Chlorophyll-*a* was likely the weakest predictor of NCP because conversions of f-chl to chl-*a* were poor and the C:Chl ratio was difficult to estimate. A more direct measure of carbon rather than chlorophyll is needed to understand biogeochemical cycles. Although the strongest slope was found between $\Delta\text{depth-integrated } c_p(660)$ and NCP_{O_2} , this is likely just a coincidence since the same slope is not seen over the day.

Since we were estimating the same quantity on both axes, we expected to obtain a 1:1 relationship for each proxy. Yet in all cases, our slope was off by a factor of ap-

proximately 5. One possibility for this discrepancy is the fact that we used total POC, c_p , and b_{bp} , which includes both living and detrital components, rather than isolating phytoplankton carbon and the attenuation and backscattering due to phytoplankton (c_{phyto} and b_{bphyto} respectively). This error would have been introduced during the initial conversion of c_p and b_{bp} to POC. In order to determine if isolating phytoplankton carbon could reasonably explain this discrepancy, we conducted a thought experiment. We estimated phytoplankton carbon (PC) after Behrenfeld et al. (2005) as a constant proportion (30%) of the total POC pool. In order to obtain a final 1:1 relationship, this would have called for 8% of c_p and 6% of b_{bp} to be attributable to phytoplankton.

These percentages may be reasonable for b_{bphyto} but it is unlikely that c_{phyto} would be that small. Durand and Olson (1996) found that 50% of beam attenuation was attributable to phytoplankton and that changes in c_p were almost completely explained by changes in c_{phyto} . On the other hand, Green et al. (2003) found that the main contributors to b_b in New England coastal shelf waters were detritus and minerals in the summer and only minerals in the spring. Upon isolating the various contributions to b_b , when taken as a percentage of b_{bp} , 44% was due to minerals, 41% was due to detritus, 9% was a result of heterotrophic prokaryotes, and eukaryotic phytoplankton and *Synechococcus* contributed 2.5% each. It is likely then that isolating b_{bphyto} would have significantly improved our 1:1 relationship, but it is unlikely to have been the case for c_{phyto} .

2.4.4 Experiment Weaknesses

Our current experiment has many weaknesses and calculations are associated with high errors, indicative that there is significant room for improvement in future ship-board experiments. To truly obtain an understanding of NCP, consecutive 24-hour measurements would be required. We do not know how nighttime respiration, air-sea

flux, and bubble injection pre-conditioned our morning casts and as such, we were unable to assess day-to-day changes in NCP. Our measurements were constrained to sunlit hours. Alternate determinations of NCP via bottle incubation are one aspect of the experiment that did not produce results. The bottle data were determined not to be representative of true NCP at depth because they were incubated on deck where they were exposed to warmer temperatures and stronger PAR, which would have been attenuated at depth.

Furthermore, many parameters required for NCP calculations were not measured and we had to rely upon the literature to find suitable estimates. In particular, an appropriate C:Chl ratio was required to convert chl-*a* into phytoplankton carbon. C:Chl ratios differ substantially among phytoplankton species (Langdon, 1987) as well as with temperature, nutrient availability, and light (Behrenfeld et al., 2005). Since phytoplankton communities change throughout the year and environmental conditions change seasonally, future experiments would benefit by taking phytoplankton samples to determine the dominant species present and determine the C:Chl ratio.

Likewise, a literature estimate of gravitational POC flux in the GoM was applied to our data. It would be informative to directly measure the gravitational POC flux via sediment traps once the euphotic depth is established. As with the C:Chl ratio, sinking rates will vary based on the phytoplankton community present, as different communities will have variable size, shape, and density which can affect sinking rates (Fischer and Karakaş, 2009).

Little is known about the extracellular release of DOC, but Marañón et al. (2004) suggests that productivity measurements are greatly underestimated if DOC production is omitted. In order to estimate the extracellular release of DOC we used the mean PER (19%) found by Marañón et al. (2004), however, this data was collected in Spain. Local measurements in the GoM were conducted by Mague et al. (1980), who found a PER of 5-10%, but Marañón et al. (2004) suggested this is an under-

estimate because DOC may have adsorbed to the GF/F filters. Additionally, only surface samples were collected and Marañón et al. (2004) found PER to increase with depth. They also showed that PER is affected by irradiance but it is unclear whether it is related to phytoplankton size. Since much uncertainty surrounds the ratio of DOC production to total carbon production, it would be better to measure DOC production directly.

Again, vertical eddy diffusivity was taken from the Benitez-Nelson et al. (2000) study in the GoM. However, eddy diffusivity has been shown to vary within the GoM by area and season (Townsend, 2002). ^7Be has been shown to provide a useful estimate of eddy diffusivity and may be more accurate than estimations from empirical models, offering a potential method of k_z measurement for future experiments.

2.4.5 Improvements for Future Experiments

Our study was brief and limited data was collected to provide a significant understanding of NCP in the western GoM. A well-designed future experiment will seek to elucidate the annual cycle of NCP in order to clarify the effects of seasonal changes in temperature, light, labile organic carbon, inorganic nutrients, and phytoplankton community. This would involve week to month-long cruises each season where samples should be taken continuously throughout the daytime and nighttime to capture diel cycles, as our data was limited by a lack of knowledge about how nighttime respiration contributes to NCP. Depth profiles should be taken every hour to provide increased temporal resolution, and independent determinations of NCP through bottle incubations should be conducted at depth to avoid the temperature and light attenuation issues seen in our experiment. Additionally, some instruments such as an optode could be situated directly on the drifter at several depths (*i.e.* surface, chlorophyll maximum, and euphotic depth) to provide continuous coverage while still allowing for the integration of the O_2 profile over the euphotic depth.

In order to minimize the errors associated with NCP calculations, as many variables as possible should be sampled directly to avoid reliance on literature values. Regular phytoplankton samples should be collected to characterize the dominant phytoplankton community and determine an appropriate C:Chl ratio. Particulate carbon could be measured through the use of an elemental analyzer and chl-*a* could be measured fluorometrically as in Langdon (1987). Seasonal gravitational fluxes could be measured through the use of a sediment trap that could be attached to the drogue so that it would drift with the water mass being traced. DOC production could be estimated following Marañón et al. (2004) through the use of simulated *in situ* incubations where seawater samples spiked with ^{14}C are incubated at the light and temperature conditions measured by the profiler. k_z can be derived through the steady-state model described by Silker (1972), which would require the collection of ^7Be on iron-impregnated filters (Benitez-Nelson et al., 2000).

Ideally, it would be advantageous to have concurrent satellite imagery of chl-*a*, b_{bp} and c_p over the cruise periods to examine whether optical parameters measured by satellite produce the same estimates for POC inventories and hence NCP as the optical parameters measured *in situ*. However, this would require a satellite being positioned above the study area in order to take closely-spaced sequential images. Presently we do not have that capability, but it may become a reality in the near future with the launch of NASA's geostationary satellite, GEO-CAPE.

2.4.6 Implications and Conclusions

This research reports on a novel method of retrieving NCP by using an optical proxy to track changes in particle inventories. Since most particles in the euphotic zone are of biological origin, it is reasonable to assume that community consumption and production can be estimated by knowledge of the temporal dynamics of particle inventories. Two of the three optical parameters examined in this study are retrievable

from satellite and can act as indices for POC. It follows then that changes in particle stocks retrieved by satellite could provide a first order estimation of NCP.

Significantly stronger relationships were seen between casts compared to over the day. Part of this may be attributable to the fact that there were fewer points over the day than between casts. However, if there is a stronger relationship over shorter time periods, this has implications for monitoring NCP by satellite. Currently, satellites such as SeaWiFS and MODIS-Aqua can only collect images once every day or two. If there is excessive cloud cover, data may only be collected once or twice a week, which is not suitable for estimating NCP because one image is not enough to give information about a rate. A rate implies a change over time, so consecutive snapshots over short periods of time to track a moving water mass and correct for advection using modelled velocity fields are necessary to estimate NCP.

NASA is planning to launch a new satellite, GEO-CAPE, that will be in geosynchronous orbit with the earth, and as such will be stationary over one area. It would be capable of capturing data on short-term time scales and could likely get a good measure of NCP. Currently a similar geostationary satellite, the COMS-GOCI, is operating above the Korean Sea. It is capable of capturing 8 daytime images and 2 nighttime images. Polar orbiters could even provide additional looks that could be combined with geostationary images.

This research presents the possibility of using optical parameters to estimate POC inventories and utilize the temporal derivative as a first order estimate of NCP. The best estimate was derived from c_p as it is dominated by particles in the phytoplankton size domain. While c_p is not currently a satellite product, it is highly desirable and greater efforts should be made to retrieve it. Strong relationships seen between casts imply the need for improved resolution of satellite images in space and time. NASA's GEO-CAPE satellite has the potential to fulfill this task. For the first time ever, we would be able to estimate the biogeochemical contribution of NCP to the carbon cycle

and be able to continually monitor the effects of climate change and anthropogenic perturbations on NCP.

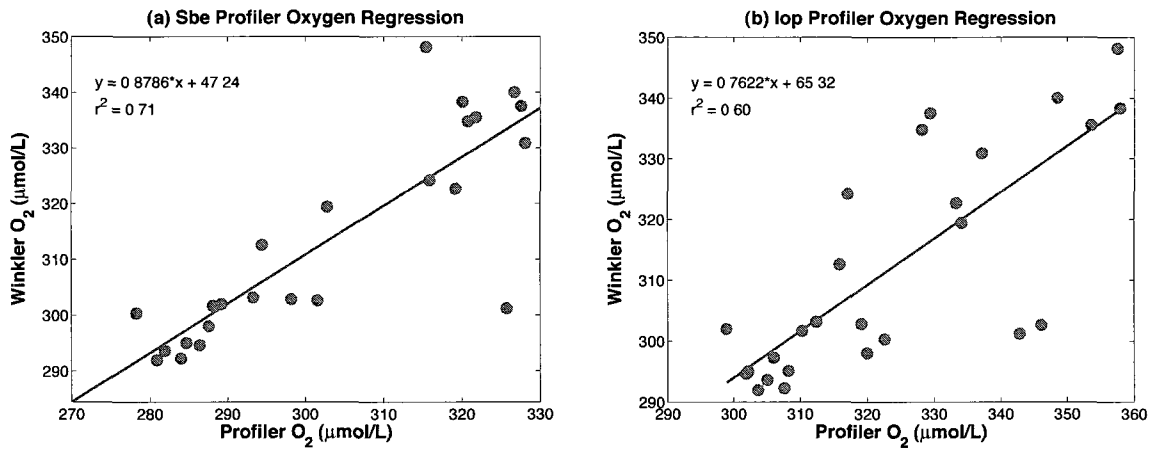


Figure 2-1: Oxygen corrections for both profilers.

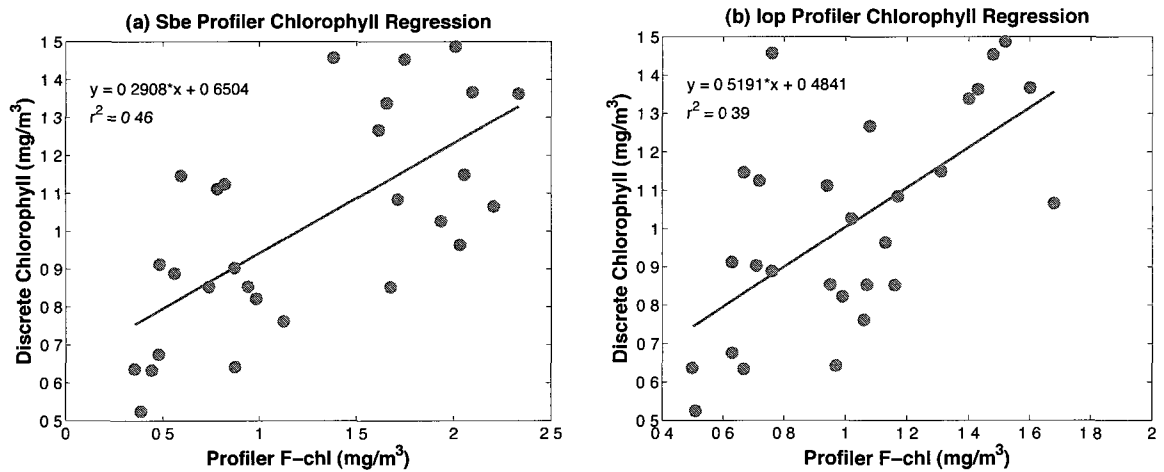


Figure 2-2: Chlorophyll corrections for both profilers.

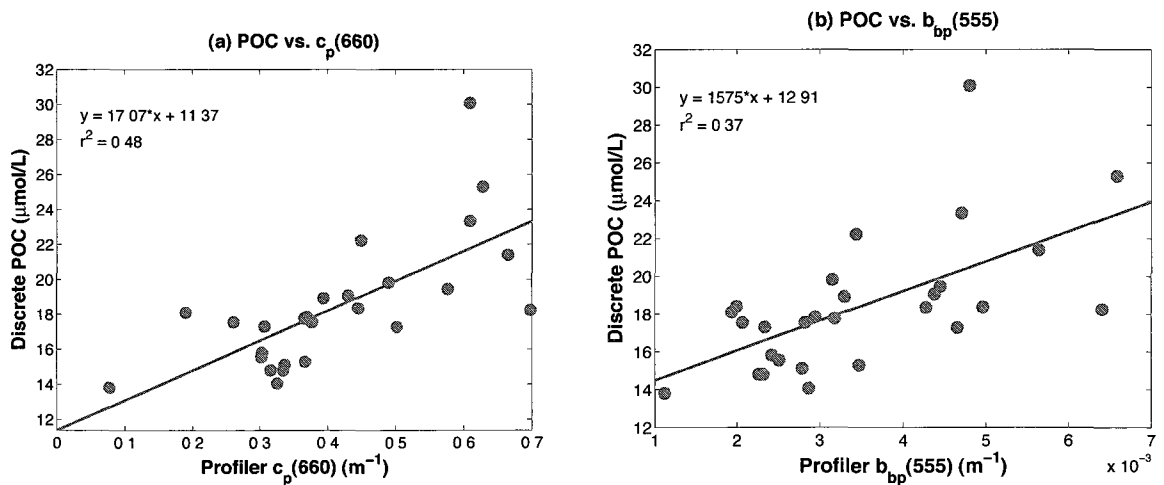


Figure 2-3: Regressions used to convert $c_p(660)$ and $b_{bp}(555)$ to POC.

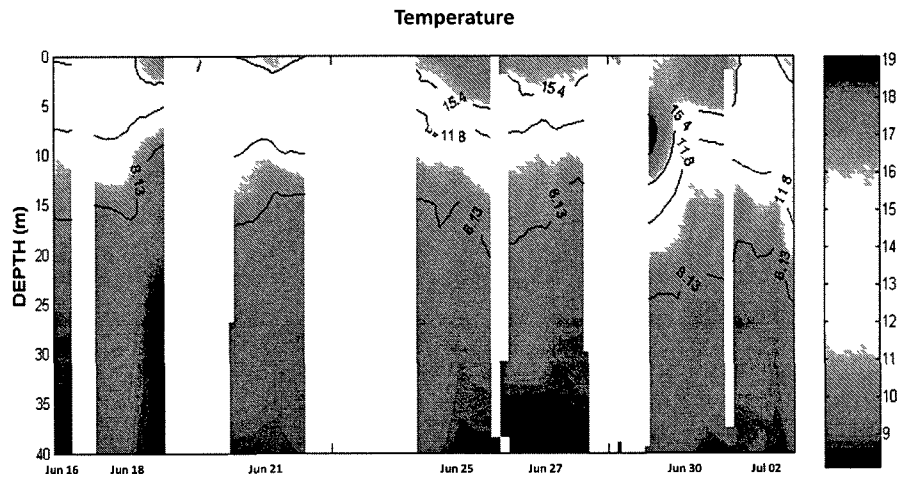


Figure 2-4: A kriged plot of temperature ($^{\circ}\text{C}$) with periods of high variance in between cruise days masked out.

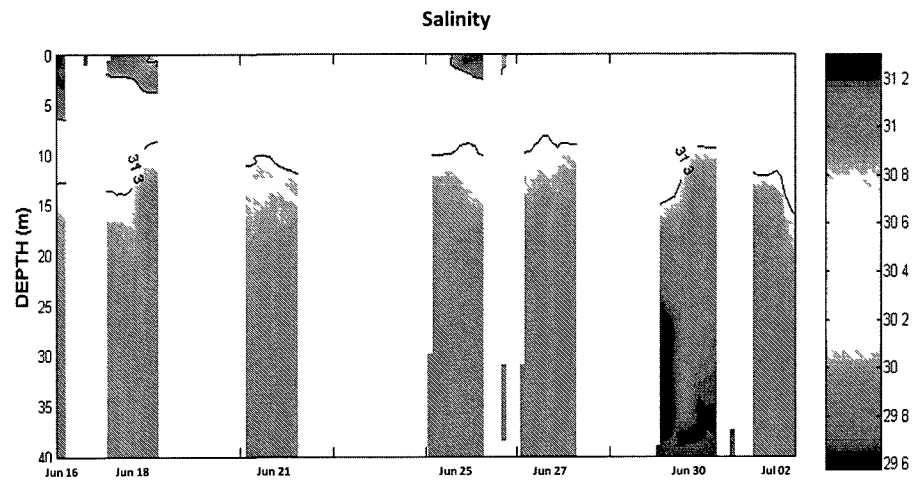


Figure 2-5: A kriged plot of salinity (psu) with periods of high variance in between cruise days masked out.

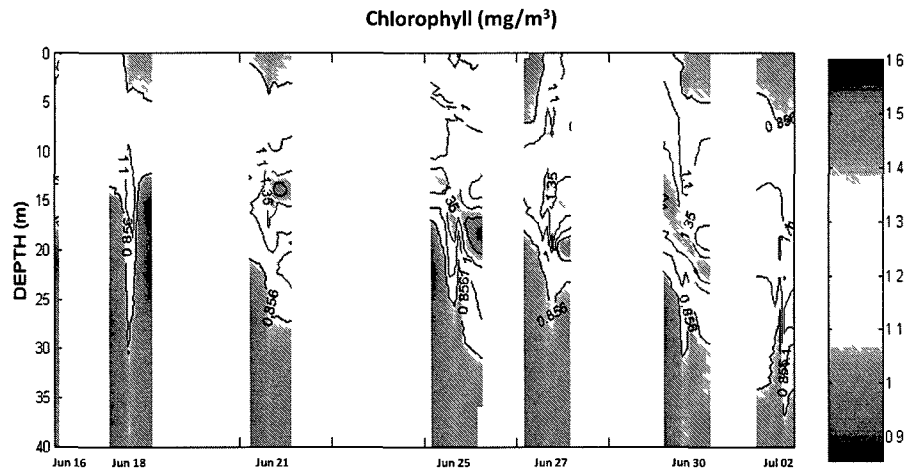


Figure 2-6: A kriged plot of f-chl (mg m^{-3}) with periods of high variance in between cruise days masked out.

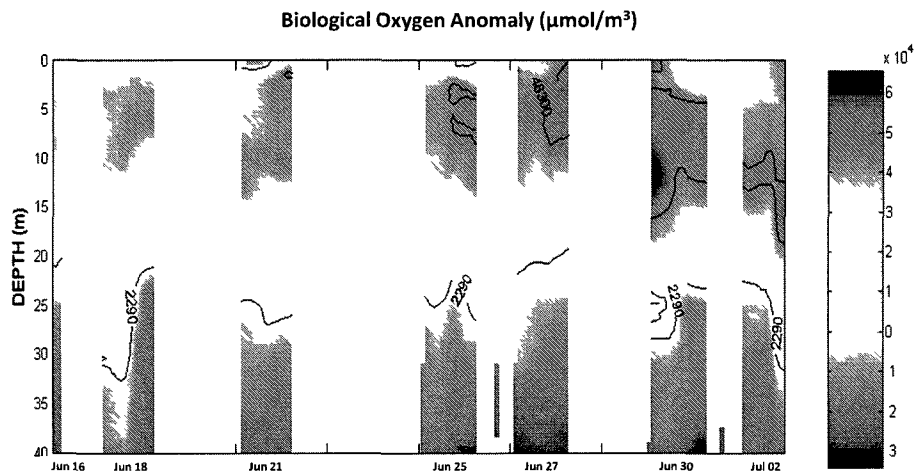


Figure 2-7: A kriged plot of the biological oxygen anomaly ($\mu\text{mol m}^{-3}$) with periods of high variance in between cruise days masked out

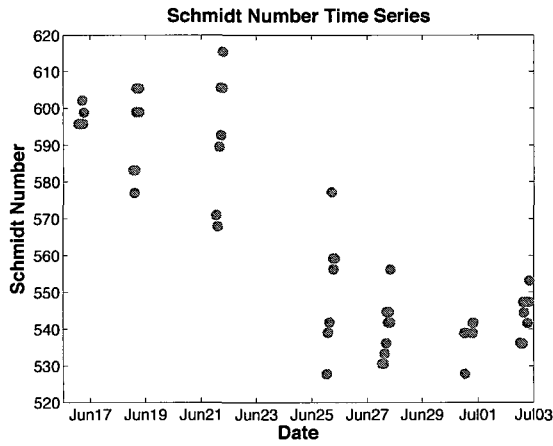


Figure 2-8: A time series plot of Schmidt numbers (dimensionless) for oxygen during the cruises. Each dot represents a cast.

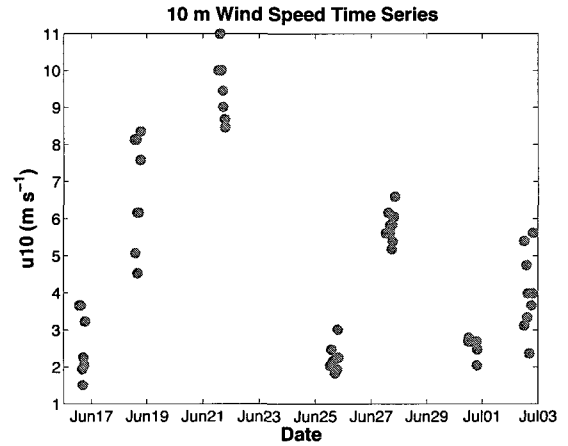


Figure 2-9: A time series plot of 10 m wind speed (u_{10}) for the cruises. Each dot represents a cast.

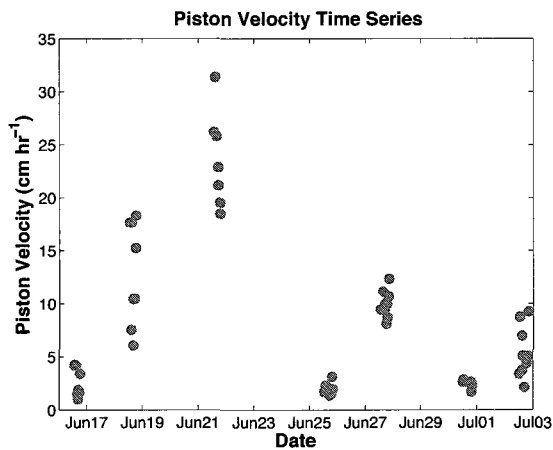


Figure 2-10: A time series plot of piston velocity (cm hr^{-1}) for the cruises. Each dot represents a cast.

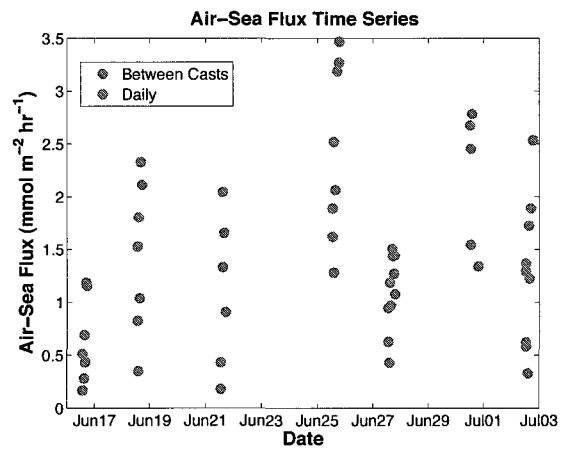


Figure 2-11: A time series plot of air-sea flux ($\text{mmol m}^{-2} \text{hr}^{-1}$) for the cruises. Blue dots represent fluxes between casts and red dots represent the flux over the course of the day (last cast minus the first cast) for both profilers.

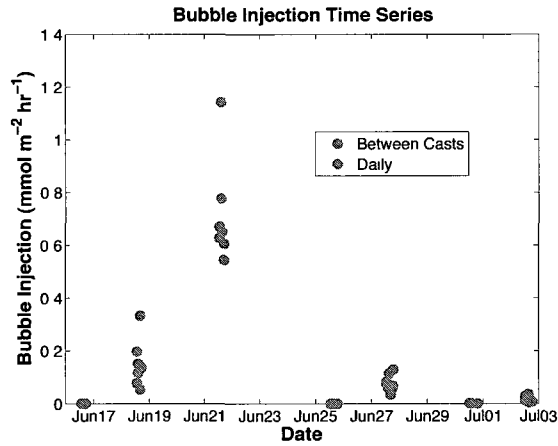


Figure 2-12: A time series plot of bubble injection ($\text{mmol m}^{-2} \text{hr}^{-1}$) for the cruises. Blue dots represent fluxes between casts and red dots represent the flux over the course of the day (last cast minus the first cast) for both profilers.

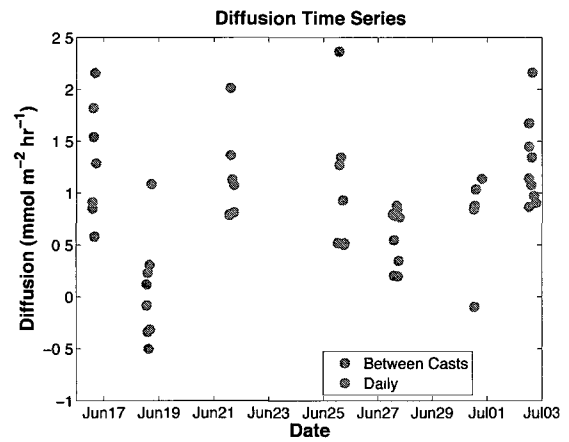


Figure 2-13: A time series plot of diffusion ($\text{mmol m}^{-2} \text{hr}^{-1}$) for the cruises. Blue dots represent fluxes between casts and red dots represent the flux over the course of the day (last cast minus the first cast) for both profilers.

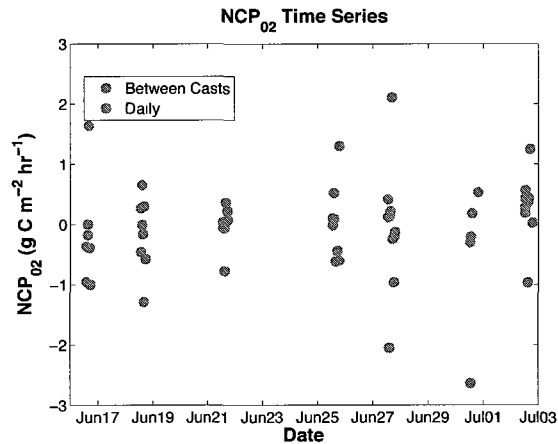


Figure 2-14: A time series plot of NCP ($\text{g C m}^{-2} \text{hr}^{-1}$) for the cruises. Blue dots represent NCP between casts and red dots represent NCP over the course of the day (last cast minus the first cast) for both profilers.

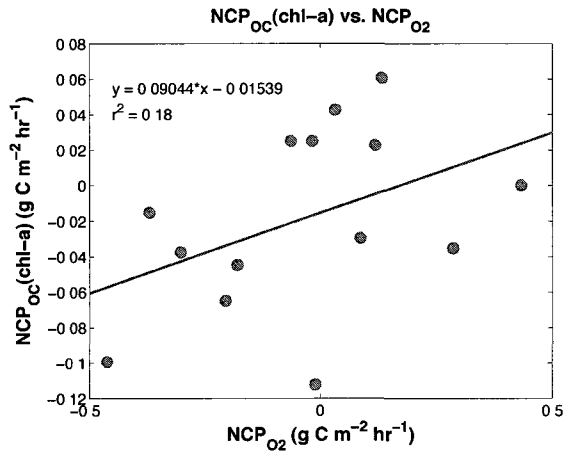


Figure 2-15: The relationship between NCP derived from chl-a (converted from f-chl) vs. NCP_{O_2} over the course of the day.

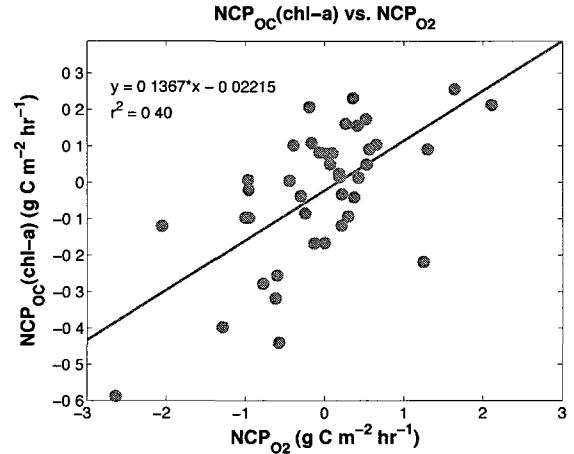


Figure 2-16: The relationship between NCP derived from chl-a (converted from f-chl) vs. NCP_{O_2} calculated between casts.

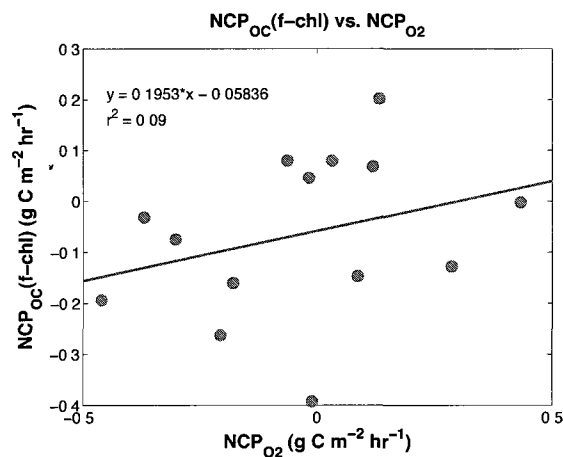


Figure 2-17: The relationship between NCP derived from uncorrected profiler f-chl vs. NCP_{O_2} over the course of the day.

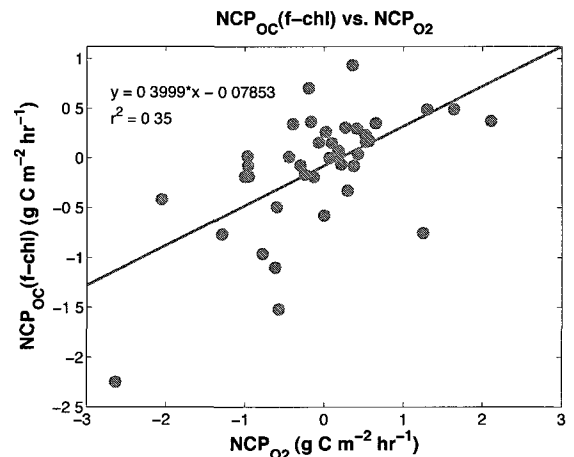


Figure 2-18: The relationship between NCP derived from uncorrected profiler f-chl vs. NCP_{O_2} calculated between casts.

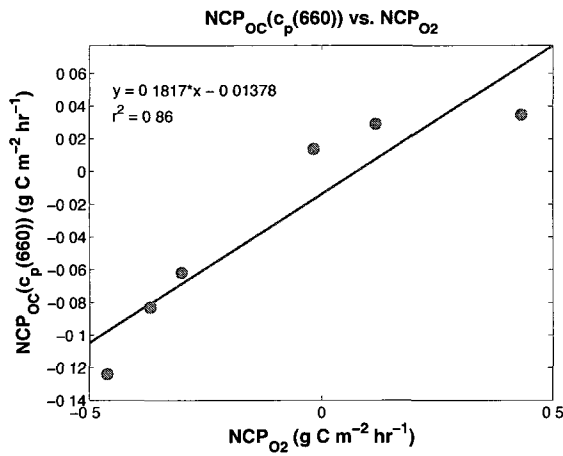


Figure 2-19: NCP derived from $c_p(660)$ vs. NCP_{O_2} over the course of the day.

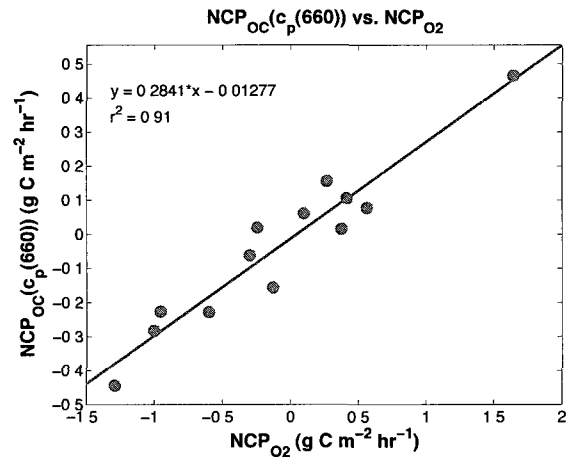


Figure 2-20: NCP derived from $c_p(660)$ vs. NCP_{O_2} calculated between casts.

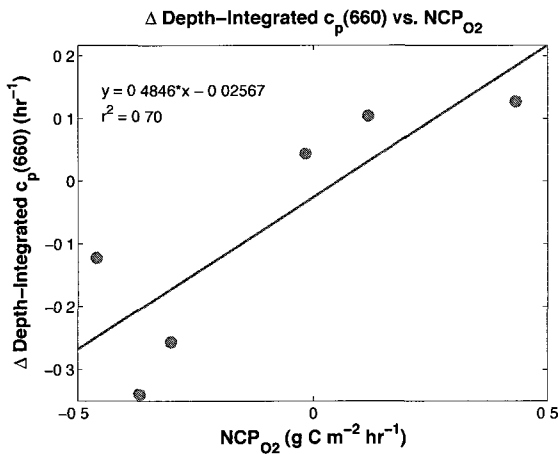


Figure 2-21: Raw $c_p(660)$ data plotted against NCP_{O_2} without converting to POC over the course of the day.

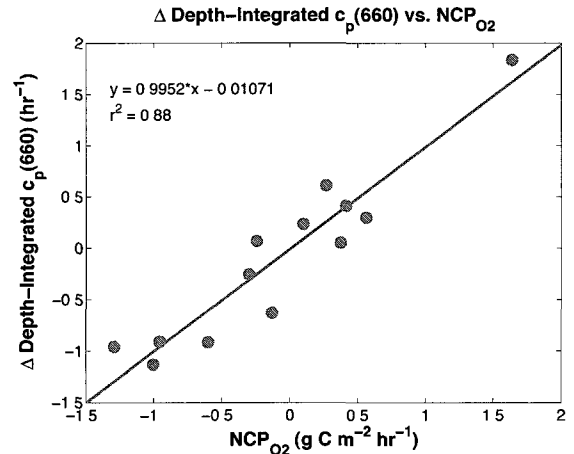


Figure 2-22: Raw $c_p(660)$ data plotted against NCP_{O_2} without converting to POC calculated between casts.

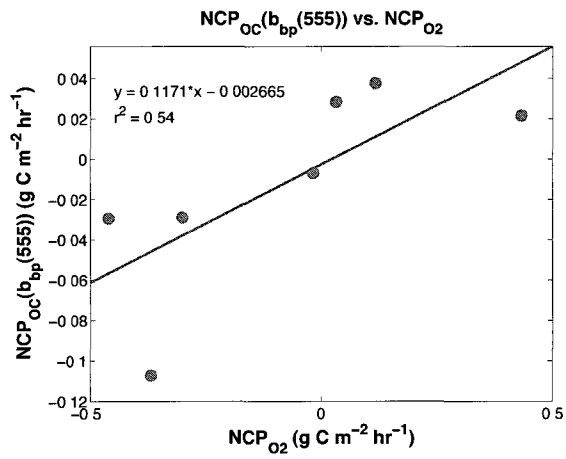


Figure 2-23: POC derived from $b_{bp}(555)$ vs. NCP_{O₂} over the course of the day.

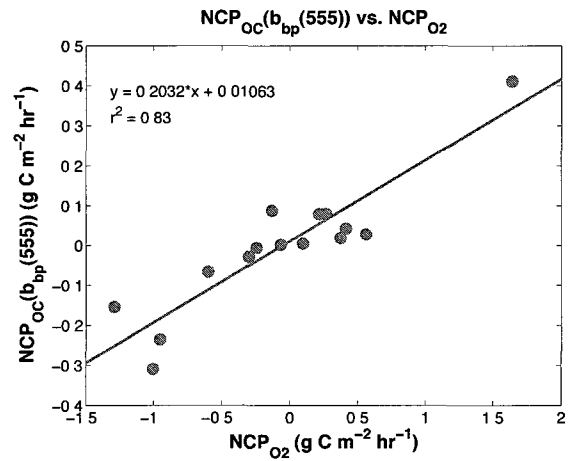


Figure 2-24: POC derived from $b_{bp}(555)$ vs. NCP_{O₂} calculated between casts.

Table 2.1: Displayed is a table of the errors associated with POC calculations. Sbe and iop refer to the two different profilers. Day and btw refer to the two different time scales analyzed (over the course of the day and between casts respectively). All means displayed are from the original data or the literature, not a Monte Carlo analysis. Standard deviations (SD) are from a Monte Carlo simulation where indicated.

	mean	SD	units	source
m (f-chl, sbe)	0.29	0.07		data
b (f-chl, sbe)	0.65	0.10	mg m ⁻³	data
m (f-chl, iop)	0.52	0.13		data
b (f-chl, iop)	0.48	0.14	mg m ⁻³	data
m (<i>c_p</i> , iop)	17.1	3.65		data
b (<i>c_p</i> , iop)	11.4	1.60	μmol L ⁻¹	data
m (<i>b_{bp}</i> , iop)	1575	401.2		data
b (<i>b_{bp}</i> , iop)	12.9	1.50	μmol L ⁻¹	data
<i>z_{eu}</i>	24.4	2.69	m	data
PER	19%	5%		Marañón et al. (2004)
ΔDOC (chl- <i>a</i> , day)	-0.0035	0.01	g C m ⁻² hr ⁻¹	Monte Carlo
ΔDOC (chl- <i>a</i> , btw)	-0.0058	0.04	g C m ⁻² hr ⁻¹	Monte Carlo
ΔDOC (<i>c_p</i> , day)	-0.0060	0.08	g C m ⁻² hr ⁻¹	Monte Carlo
ΔDOC (<i>c_p</i> , btw)	-0.0072	0.16	g C m ⁻² hr ⁻¹	Monte Carlo
ΔDOC (<i>b_{bp}</i> , day)	-0.0023	0.01	g C m ⁻² hr ⁻¹	Monte Carlo
ΔDOC (<i>b_{bp}</i> , btw)	-5.93e ⁻⁴	0.03	g C m ⁻² hr ⁻¹	Monte Carlo
<i>F_g</i>	3.09	1.55	μmol m ⁻² s ⁻¹	Packard and Christensen (2004)
NCP (chl- <i>a</i> , day)	-0.019	0.05	g C m ⁻² hr ⁻¹	Monte Carlo
NCP (chl- <i>a</i> , btw)	-0.031	0.18	g C m ⁻² hr ⁻¹	Monte Carlo
NCP (<i>c_p</i> , day)	-0.032	0.39	g C m ⁻² hr ⁻¹	Monte Carlo
NCP (<i>c_p</i> , btw)	-0.038	0.81	g C m ⁻² hr ⁻¹	Monte Carlo
NCP (<i>b_{bp}</i> , day)	-0.012	0.05	g C m ⁻² hr ⁻¹	Monte Carlo
NCP (<i>b_{bp}</i> , btw)	-0.0032	0.16	g C m ⁻² hr ⁻¹	Monte Carlo

Table 2.2: Displayed is a table of the errors associated with O₂ calculations. Sbe and iop refer to the two different profilers. Day and btw refer to the two different time scales analyzed (over the course of the day and between casts respectively). All means displayed are from the original data or the literature, not a Monte Carlo analysis. Standard deviations (SD) are from a Monte Carlo simulation where indicated.

	mean	SD	units	source
m (O ₂ , sbe)	0.88	0.12		data
b (O ₂ , sbe)	47.2	35.7	$\mu\text{mol L}^{-1}$	data
m (O ₂ , iop)	0.76	0.13		data
b (O ₂ , iop)	65.3	41.2	$\mu\text{mol L}^{-1}$	data
[O ₂] _{sat}	profile	0.015	mL L^{-1}	Weiss (1970)
z_{eu}	24.4	2.69	m	data
k	8.46	12%	cm hr^{-1}	data and Jiang et al. (2008)
k_z	1.5	0.40	$\text{cm}^2 \text{s}^{-1}$	Benitez-Nelson et al. (2000)
F_s (day)	1.52	2.00	$\text{mmol m}^{-2} \text{hr}^{-1}$	Monte Carlo
F_s (btw)	1.48	2.24	$\text{mmol m}^{-2} \text{hr}^{-1}$	Monte Carlo
F_{inj} (day)	0.14	12%	$\text{mmol m}^{-2} \text{hr}^{-1}$	data
F_{inj} (btw)	0.13	12%	$\text{mmol m}^{-2} \text{hr}^{-1}$	data
F_d (day)	0.89	0.70	$\text{mmol m}^{-2} \text{hr}^{-1}$	Monte Carlo
F_d (btw)	0.87	0.76	$\text{mmol m}^{-2} \text{hr}^{-1}$	Monte Carlo
NCP (O ₂ , day)	-0.04	0.25	$\text{g C m}^{-2} \text{hr}^{-1}$	Monte Carlo
NCP (O ₂ , btw)	-0.07	0.89	$\text{g C m}^{-2} \text{hr}^{-1}$	Monte Carlo

CHAPTER 3

INCUBATION STUDY

This experiment sought to characterize NCP in the Piscataqua Estuary Inlet and collect a long-term data set of gross primary production, respiration, and net community production rates. In order to undertake this goal, a novel incubation instrument was developed and subsequently deployed at a marine station adjacent to the Piscataqua Estuary Inlet. This system is advantageous because the incubation chambers are much larger than traditional bottle incubations and we are able to control some of the variables such as light, the length of the incubation, and to some extent temperature. Additionally, this system is capable of continuous automated measurements that would otherwise require a lot of manpower to collect. It will also provide a large data set of respiration measurements giving us information on the heterotrophic contribution to NCP, which is lacking in the literature. We hypothesize that there will be seasonal variability of NCP as phytoplankton communities evolve and inorganic nutrient and organic carbon availability changes.

3.1 Site Description

The study site is the Piscataqua Estuary Inlet, which is located along the New Hampshire-Maine border at the confluence of the Great Bay-Piscataqua estuary system and the Gulf of Maine. The Great Bay Estuary is a tidally-dominated, well-mixed system, consisting of Little Bay and Great Bay (Bilgili et al., 2005). It receives drainage from seven rivers, the Lamprey, Squamscott, Winnicut, Bellamy, Oyster, Cochecho, and Salmon Falls rivers, although their net contribution is less than 2% of

the tidal prism (Bilgili et al., 2005). The Great Bay Estuary undergoes semi-diurnal tidal exchange with the Gulf of Maine via the Piscataqua River. The island of New Castle is situated in the Piscataqua Estuary where the Piscataqua River connects to the Gulf of Maine, forming the Piscataqua Estuary Inlet (Fig. 3-1a). The sampling station for this study is the University of New Hampshire's Coastal Marine Lab (CML), which is located in the old Mines building of historic Fort Constitution on the Fort Point Peninsula in New Castle, NH (Fig. 3-1b).

Previous work in the Piscataqua Estuary Inlet by Brown (2006) found that during low tide, water measured at the inlet was uncontaminated Piscataqua Estuary water and during high tide, the water was essentially near-shore western GoM water. Brown (2006) also investigated oxygen dynamics and attributed its variability to both physical and biological controls. He concluded that the biological activity appeared to be ocean driven rather than estuary driven and warranted further study. Therefore, we propose to use a novel incubation instrument to collect continuous production and respiration data to elucidate the annual magnitude and diurnal variability of NCP and the contribution of phytoplankton community dynamics.

3.2 Methods

3.2.1 Data Collection

Data for this study were collected at the Coastal Marine Lab (CML) adjacent to the Piscataqua Estuary Inlet. The lab houses a flow-through water pump that distributes seawater throughout the facility. The intakes are located about 20 m out into the Inlet and 0.5 m from the bottom. This puts the intakes roughly 6 m from the surface at high tide and 3.5 m at low tide (Brown, 2006). Two large impeller pumps each draw in seawater at a rate of 570 liters per minute pumping it 70 m into the facility to the header tanks, although only one pump is in use at a time. Seawater is

then distributed to the facility from the header tanks.

For our experiment, one tank was installed with a suite of instruments to measure the initial properties of the seawater as it was pumped in (Fig. 3-2). Absorption and beam attenuation at nine wavelengths (ac-9, WET Labs), turbidity, chlorophyll, and colored dissolved organic matter (Triplet, WET Labs), pCO₂ (equilibrator, Idrysis), dissolved oxygen (Optode, Aanderaa), and temperature, conductivity, and salinity (CT, Aanderaa) were measured. In order to incubate water, we utilized a novel custom-built, autonomous dual-chamber instrument (Langdon Enterprises) that automatically sampled and incubated seawater to measure changes in dissolved oxygen (Fig. 3-3). The instrument consists of two 16-liter transparent polycarbonate chambers. It was important that they were not made from acrylic plastic, which contains UV stabilizing compounds capable of reacting with the oxygen in the water. One chamber was darkened with aluminum foil in order to provide a dark environment for respiration to occur. The other chamber was left clear so light could penetrate the chamber for photosynthesis. A multispectral light source (D-D Midday 6000 T5HO, Giesemann) was installed above to provide the light needed for photosynthesis. Both chambers were equipped with an optode to measure dissolved oxygen and temperature (Optode 4835, Aanderaa) and stirring rods to keep the water well mixed. Additionally, the light chamber contained a PAR sensor (QSL, Biospherical) to measure light from all directions. The light chamber was also wrapped with clear hosing through which cool water was pumped to keep the chamber from heating significantly more than the dark chamber. Each chamber has an inflow and outflow line at the bottom, and an overflow line at the top. Solenoid valves were programmed to pump and drain seawater into and out of the chambers. A two-chamber settling tank was constructed to filter out sediment as seawater was pumped in for incubation (Fig. 3-4). Incubations were conducted at high tide from June through September in varying increments from 3-12 hours. The instrument was cleaned with a 5% bleach

solution when necessary.

3.2.2 Data Processing

Oxygen data from the optodes were utilized to calculate the biological oxygen anomaly. First, the raw optode data were processed according to Aanderaa specifications to correct for salinity. An additional adjustment was applied to correct for the offset between the optodes in each chamber. Then the expected oxygen at saturation was calculated according to Weiss (1970) and subtracted from the observed oxygen in order to get the biological oxygen anomaly. NCP was calculated as the difference between the beginning and ending biological oxygen concentration over the length of the incubation in the light chamber. Similarly, the rate of respiration was the difference in the biological oxygen over the course of the incubation in the dark chamber. The rate of gross primary production was determined by summing respiration and NCP.

3.3 Results

The results of our incubations fell into three general patterns. Several incubations representative of each category will be presented. The first pattern observed was an expected production and respiration pattern (Fig. 3-5). Data is presented from June 28 to July 5, 2011. In all incubations, production was observed in the light chamber while respiration was observed in the dark chamber. Late June incubations had small rates of production ($\leq 5 \mu\text{mol O}_2 \text{ L}^{-1}$) while July rates saw a large increase to $>15 \mu\text{mol O}_2 \text{ L}^{-1}$. Respiration rates saw a slight increase as well. Over the course of the incubation, temperatures saw an increase of about 5 °C but the temperatures in each chamber remained fairly close together with only a 1-2 °C difference (Fig. 3-6). PAR levels were constant for the first six incubations and dropped slightly for

the last three, likely due to the chambers becoming dirty (Fig. 3-7). The PAR data tended to show a decrease over the course of the incubation, perhaps from increased light attenuation as particulate matter accumulated. The PAR data exhibited an unexpected shape for all incubations that will be addressed in the next section.

The second pattern observed was a lack of production in the light chamber (Fig. 3-8). In most of these eight incubations from June 21 to June 27, 2011, the light chamber data mirrored the dark chamber data showing little to no production. It is possible that this occurred due to biofouling in the pipes carrying water to our chambers. Once the pipes were cleaned out, data returned to expected results. Temperature differences between the chambers were slightly greater as the hose cooling the light chamber became clogged with organisms reducing water flow (Fig. 3-9). PAR stayed more constant during the incubation since no production occurred to increase light attenuation (Fig. 3-10).

Production in the dark chamber was the final pattern exhibited (Fig. 3-11). In each of these nine incubations, production in the light chamber was extremely high (25-35 $\mu\text{mol O}_2 \text{ L}^{-1}$). Respiration began equally strong, but about three quarters of the way through the incubation, production suddenly began occurring in the dark chamber. Temperatures stayed between 1-2 $^{\circ}\text{C}$ apart, and increased between 4-7 $^{\circ}\text{C}$ during the incubation (Fig. 3-12). During the first five incubations, PAR decreased throughout the incubation but during the last four, it increased (Fig. 3-13). Overall PAR levels were between 40-50 $\mu\text{E m}^{-2} \text{ s}^{-1}$ which is somewhat lower than the roughly 60 $\mu\text{E m}^{-2} \text{ s}^{-1}$ that they had been previously. This is possibly due to increased light attenuation from the large rates of production seen during these incubations, biofouling of the chamber, or photon flux in the lights.

Gross primary production, respiration, and NCP rates from June 28 to August 19, 2011 are presented in Fig. 3-14. Questionable data where no production was obtained in the light chamber or production occurred in the dark chamber were excluded.

Oxygen was converted to units of carbon using the Redfield photosynthetic quotient. GPP rates ranged from about 0.46-6.29 $\mu\text{mol C L}^{-1} \text{ hr}^{-1}$. Respiration rates were small ranging from 0.19-1.07 $\mu\text{mol C L}^{-1} \text{ hr}^{-1}$. NCP values ranged from 0.03-5.68 $\mu\text{mol C L}^{-1} \text{ hr}^{-1}$. Average GPP, respiration, and NCP rates were 2.37, 0.53, and 1.84 $\mu\text{mol C L}^{-1} \text{ hr}^{-1}$, respectively. In all cases, the system was autotrophic.

3.4 Discussion

3.4.1 Initial Problems

Originally it was hoped that a large data set could be collected over the course of a year to capture seasonal variability in NCP. Unfortunately, due to delays in the construction of the instrument and several problems discovered upon its arrival, we were unable to begin collecting data until June of 2011. We experienced leaking chambers, mixing rods that would not spin, overheating solenoids, and a bug in the program. The chambers were leaking in two places: around the edges and through the bottom where the instruments were inserted. The leakage around the edges was the result of overtightening the screws fastening down the chambers and was easily fixed. The leakage through the bottom of the chambers where the instruments were was the result of missing O-rings. The mixing rods' inability to spin was caused by a wiring error. One solenoid that continually overheated was sent out to be modified. The bug in the program occurred when we tried to run incubations past midnight and so the program had to be altered.

3.4.2 GPP, Respiration, and NCP Rates

GPP, respiration, and NCP rates for cases of good data were reasonable and fell within literature values reported in other estuaries using incubation methods. Caffrey et al. (1998) measured respiration rates through dark bottle incubations in San

Francisco Bay, CA and found rates of 0-0.92 $\mu\text{mol C L}^{-1} \text{ hr}^{-1}$. Similarly, Fourqurean et al. (1997) also calculated average annual dark bottle respiration of 0.51 $\mu\text{mol C L}^{-1} \text{ hr}^{-1}$ in Tomales Bay, CA. In Long Island Sound, Goebel and Kremer (2007) found average community respiration to be 1.07 $\mu\text{mol C L}^{-1} \text{ hr}^{-1}$ through dark bottle respiration. On the continental shelf of Georgia, summer respiration ranged from 0.49-0.68 $\mu\text{mol C L}^{-1} \text{ hr}^{-1}$ found by 24 hour deck incubations (Jiang et al., 2010). These rates all correspond well to our average respiration rate of 0.53 $\mu\text{mol C L}^{-1} \text{ hr}^{-1}$.

In West Florida coastal waters, Hitchcock et al. (2010) conducted 12 hr incubations during a harmful algal bloom dominated by *Karenia brevis* and found GPP rates between 0.64-3.84 $\mu\text{mol C L}^{-1} \text{ hr}^{-1}$ and NCP rates of 0.32-1.34 $\mu\text{mol C L}^{-1} \text{ hr}^{-1}$. Russell and Montagna (2007) used open water methods to study ecosystem metabolism in the western Gulf of Mexico estuaries and found GPP of 1.5-3 $\mu\text{mol C L}^{-1} \text{ hr}^{-1}$ and net metabolism of 0 to -3.5 $\mu\text{mol C L}^{-1} \text{ hr}^{-1}$ during the summer at four estuaries. These rates are similar in magnitude to our average GPP of 2.37 $\mu\text{mol C L}^{-1} \text{ hr}^{-1}$ and average NCP of 1.84 $\mu\text{mol C L}^{-1} \text{ hr}^{-1}$.

3.4.3 No Production

There are several possible explanations for the lack of production seen in some incubations. There may have been a deficiency in nutrients required for photosynthesis to occur. Also, there may have been no viable phytoplankton community or they have been poisoned and died from residual bleach in the chambers after cleaning. This is unlikely though because the heterotrophic community was still active and poison would have killed both the autotrophic and heterotrophic communities. The most likely explanation could be that biofouling in the pipes bringing water to the incubation instrument created a dominant heterotrophic environment that used up all the nutrients and consumed the phytoplankton.

3.4.4 Dark Production

Production in the dark chamber was unexpected, but we are not the first to observe this phenomenon. Similar data were found with a light/dark Niskin bottle *in situ* incubation system at Woods Hole, MA (Van Mooy, personal communication). Other previous studies have also reported oxygen production in the dark (Riley, 1941; Dugdale and Wallace, 1960). There are several reasons that production may have been seen in the dark chamber. The first is that light may have entered the chamber providing just enough for photosynthesis to occur. However, this is unlikely since no adjustments were made to the covering on the dark chamber and subsequent incubations returned to normal respiration. Another possibility is that an air leak in the chamber caused an exchange of O_2 with the atmosphere. We do not have any way to quantify this so it is possible that a small amount of O_2 was diffusing into the chambers.

The primary assumption of light/dark incubations is that the only process affecting oxygen in the dark is respiration. A recent theory suggests that oxygen concentrations can also be affected by H_2O_2 decomposition into O_2 (Pamatmat, 1997). H_2O_2 is naturally present in surface ocean water at concentrations of 10-200 nM (Van Baalen and Marler, 1966). Additionally, several studies have found that H_2O_2 can actually be produced in the dark by phytoplankton species (Palenik et al., 1987; Palenik and Morel, 1988). In the Sargasso Sea, Palenik and Morel (1988) saw H_2O_2 production occur in dark incubations at a maximum rate of 11 nM hr^{-1} , where production of H_2O_2 was usually greatest during the first 1-2 hours. Catalase, which is present throughout the ocean, is responsible for decomposing H_2O_2 into O_2 . Experiments by Moffett and Zafriou (1990) showed an increase in O_2 caused by the decay of H_2O_2 of 14 nM during a 7-hour dark incubation. Pamatmat (1997) conducted further studies with concurrent dark incubations where one sample had been poisoned with mercuric chloride to prevent biological activity while the other remained live. The live samples

showed a drawdown of O_2 , but the poisoned samples had an O_2 increase suggesting that respiration masks the effects of O_2 production from H_2O_2 decay. However, it remains unclear as to whether this could be the case with our data. We observed an increase of O_2 on the order of several micromoles, but the literature suggests an O_2 increase of nanomoles. Even though coastal waters may have much higher concentrations of DOC, the substrate for peroxide production, it is still unlikely that this would be enough to produce the micromolar O_2 increases we sometimes measured.

3.4.5 PAR Pattern

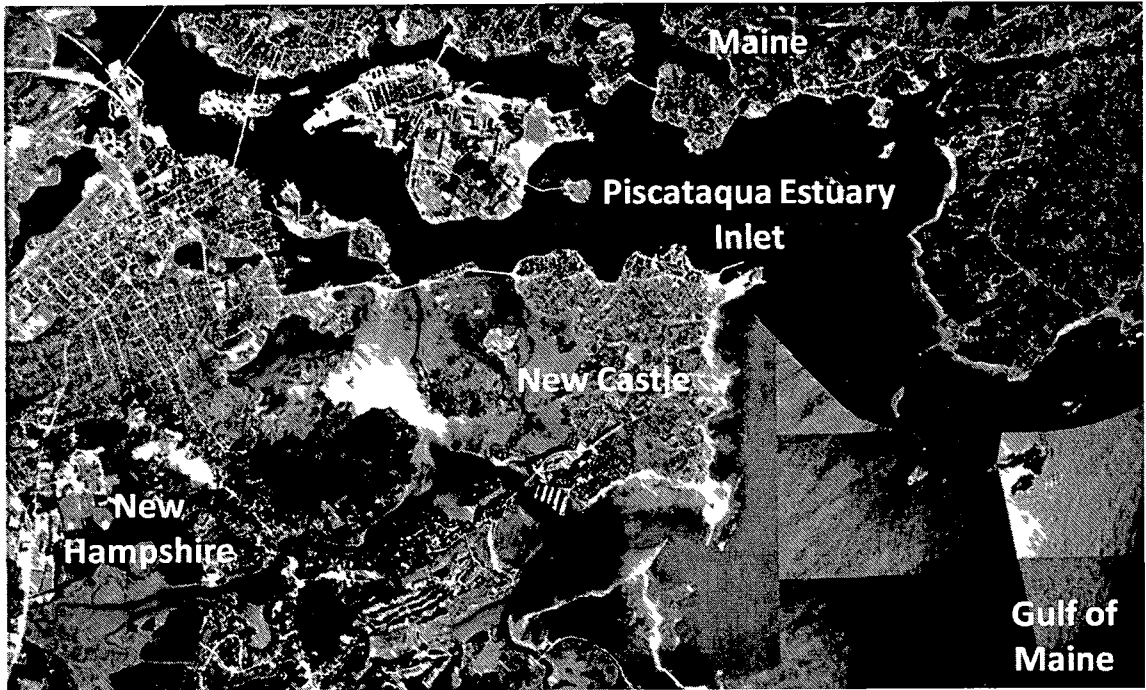
The pattern of the PAR data over the length of the incubation was unanticipated as well. It was expected that the PAR values would be fairly constant throughout the incubation. Instead, they started out high and dropped about $15 \mu E m^{-2} s^{-1}$ over the first 90 minutes of each incubation. The most likely explanation for this is that after the incubation began, condensation began to form on the outside of the chamber until the chamber was completely covered in water droplets after 90 minutes. The water droplets would have increased the scattering of light causing the gradual reduction that we see in PAR. However, the gradual decrease in PAR does not seem to have affected production and respiration rates as they look to be constant over the course of the incubation.

3.5 Improvements and Future Experiments

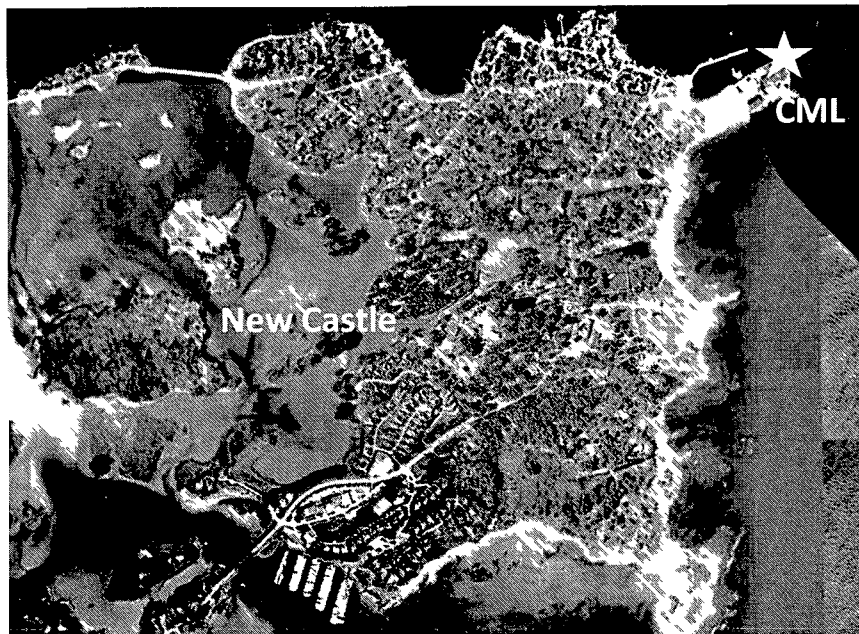
We were only able to collect a small data set and were not able to accumulate winter data or examples of community changes. Additionally, we did not have corresponding nutrient or chlorophyll data because the instruments were malfunctioning so it is difficult to explain why some incubations had much greater production than others. Although only a small data set was collected, this novel incubation chamber

had some strengths and shows promise for future work. It is automated allowing for continuous measurements with the potential to build a substantial database of GPP, NCP, and respiration rates, which are of particular interest as little respiration data exists.

Several improvements could be made to the instrument such as a better system of maintaining a constant temperature in the chambers. It is unlikely that the temperature would increase as much as it did under *in situ* conditions and increases in temperature can enhance respiration rates. Additionally, a PAR sensor inside the dark chamber would be beneficial to ensure that it has been adequately darkened. Year-round incubations should be conducted in order to understand seasonal variability in NCP caused by inorganic nutrients, labile organic carbon, and light fluctuations as well as to understand the effects of changing phytoplankton communities. Future work could also experiment with different incubation lengths and variable light conditions to simulate various *in situ* conditions. It would be beneficial to take discrete samples during incubations to be analyzed for nutrients, chlorophyll, and the dominant phytoplankton community in order to better understand the drivers of NCP variability.



(a) Piscataqua Estuary Inlet



(b) CML on the island of New Castle

Figure 3-1: The Coastal Marine Lab on the island of New Castle, located at the confluence of the Piscataqua River and the Gulf of Maine

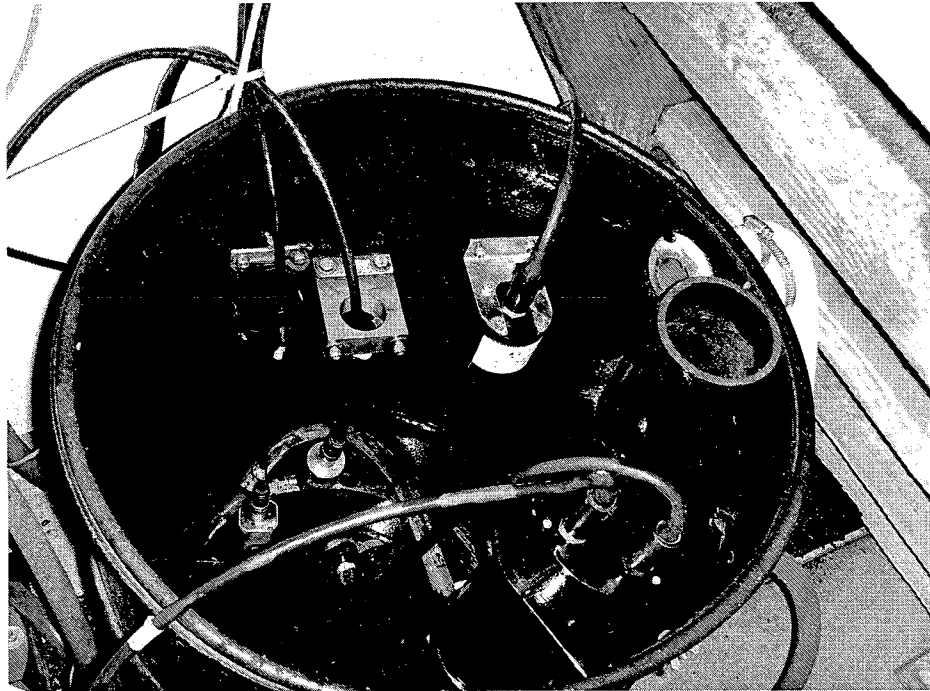


Figure 3-2: The main tank next to the incubation chamber that measures the incoming properties of the water.

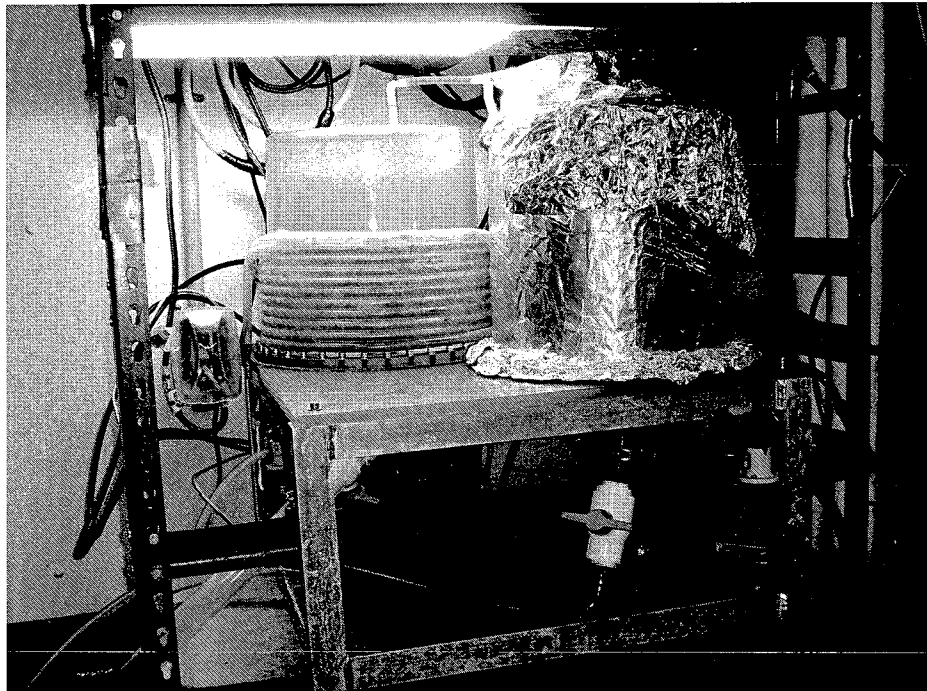


Figure 3-3: The incubation chamber custom built by Langdon Enterprises. The light chamber is on the left with a cooling hose wrapped around it. The dark chamber is covered in foil on the right. Above is a multispectral light source.

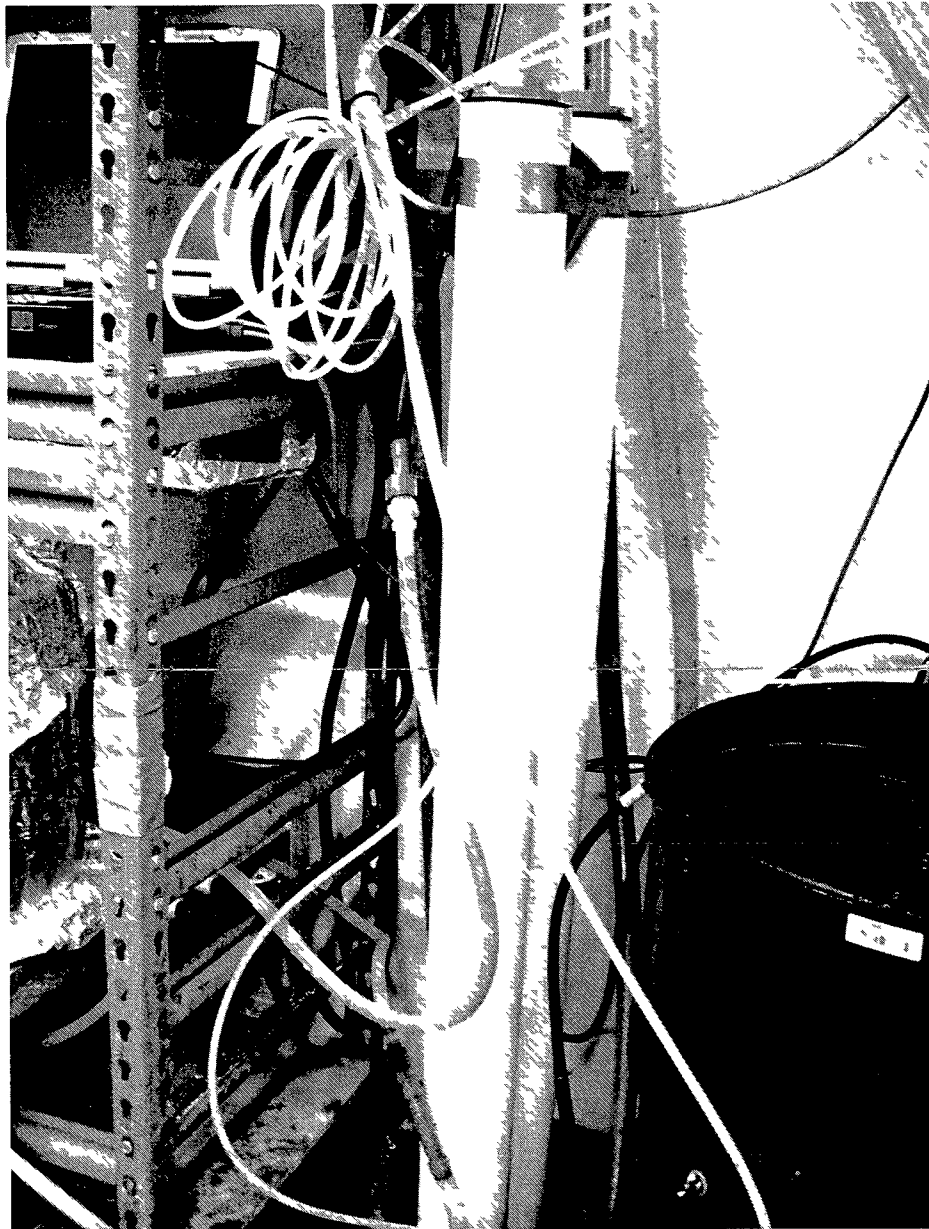


Figure 3-4: A two-chamber setting tank allowing suspended solids to settle out before water enters the incubation chambers

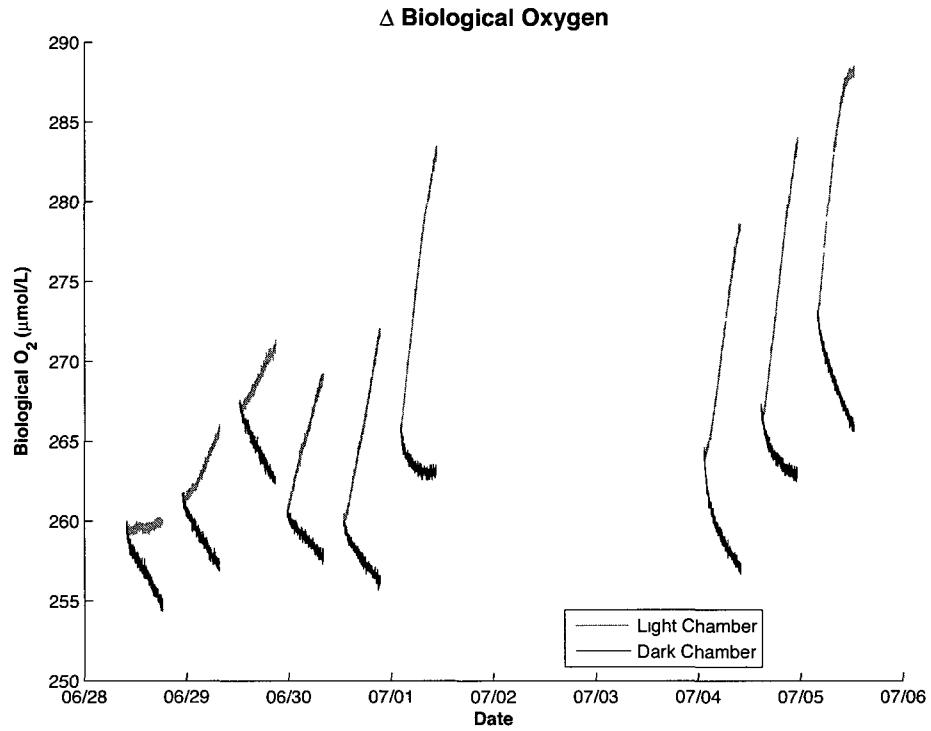


Figure 3-5: This figure shows the change in biological oxygen in each chamber during a series of 9 incubations where both respiration and NCP values were reasonable.

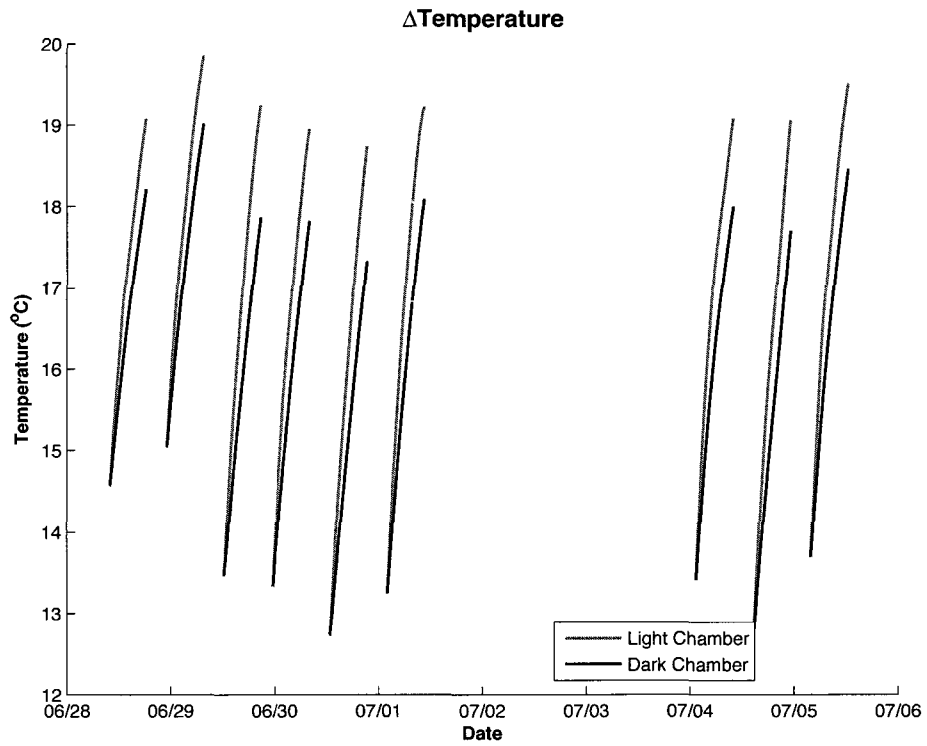


Figure 3-6: This figure shows temperature in both chambers during a series of 9 incubations where reasonable data was collected.

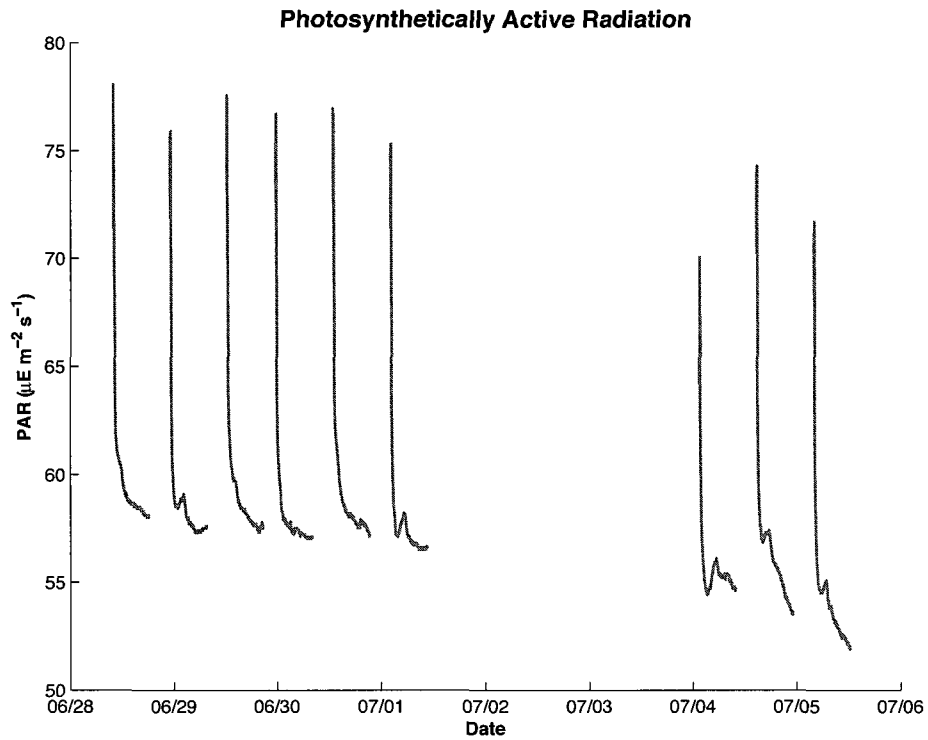


Figure 3-7: This figure shows PAR during a series of 9 incubations where reasonable data was collected. The red area highlights questionable PAR data.

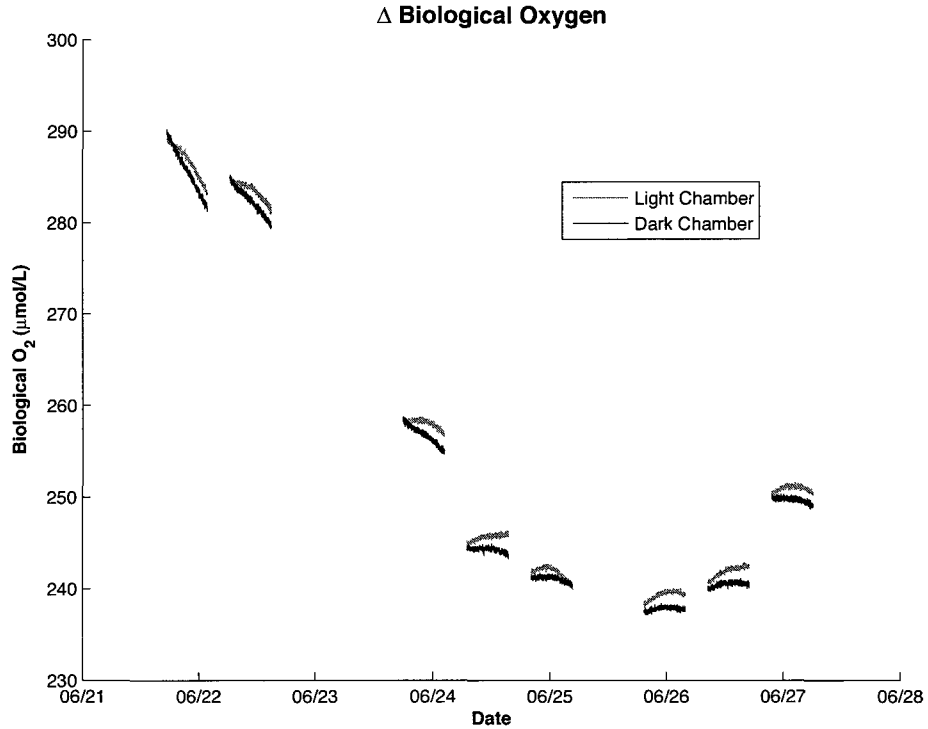


Figure 3-8: This figure shows the change in biological oxygen in each chamber during a series of 8 incubations where no production in the light chamber occurred.

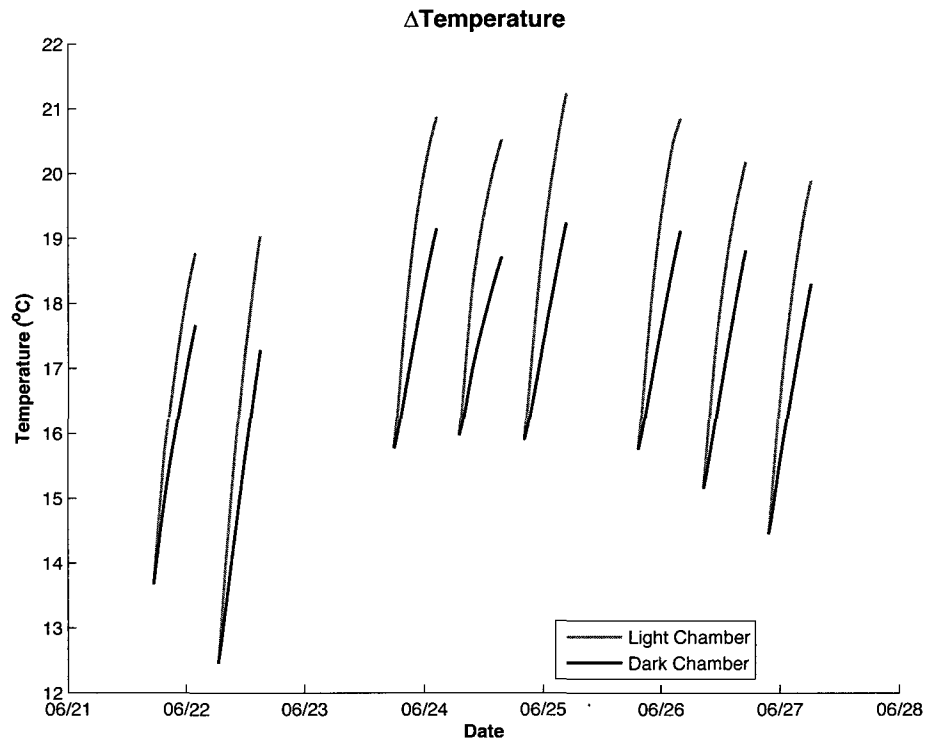


Figure 3-9: This figure shows temperature in each chamber during a series of 8 incubations where no production in the light chamber occurred.

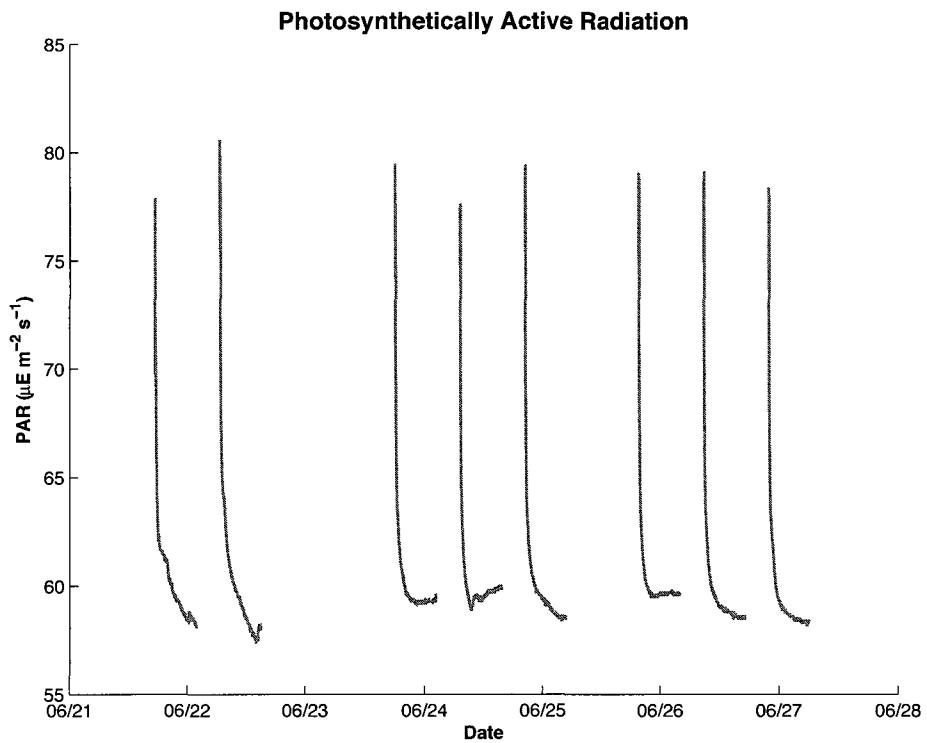


Figure 3-10: This figure shows PAR during a series of 8 incubations where no production in the light chamber occurred. The red area highlights questionable PAR data.

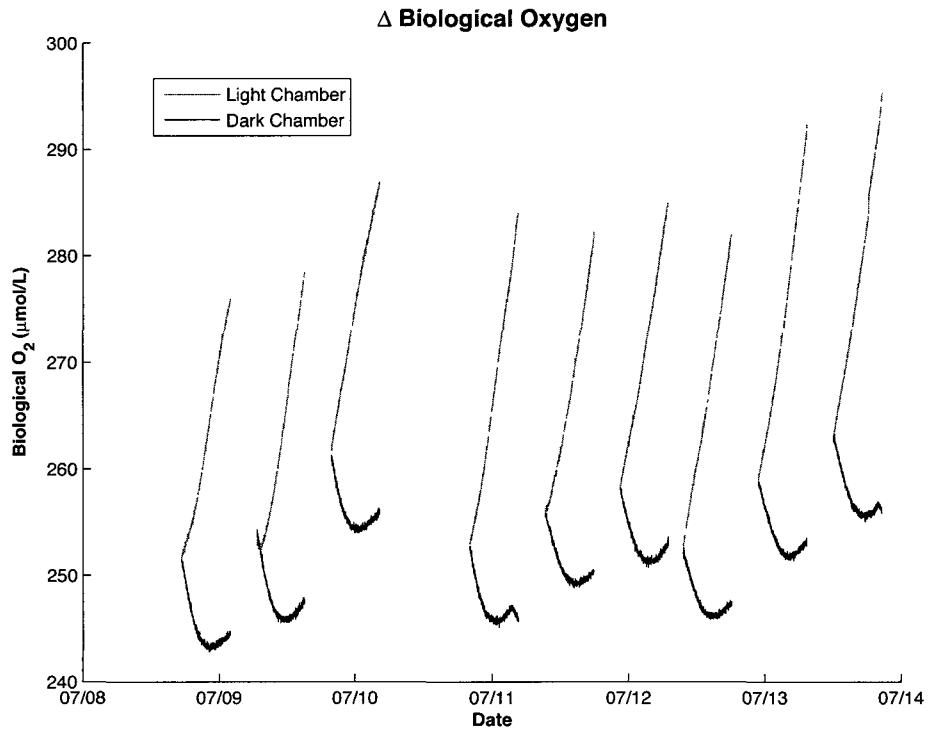


Figure 3-11: This figure shows the change in biological oxygen in each chamber during a series of 9 incubations that resulted in questionable respiration data.

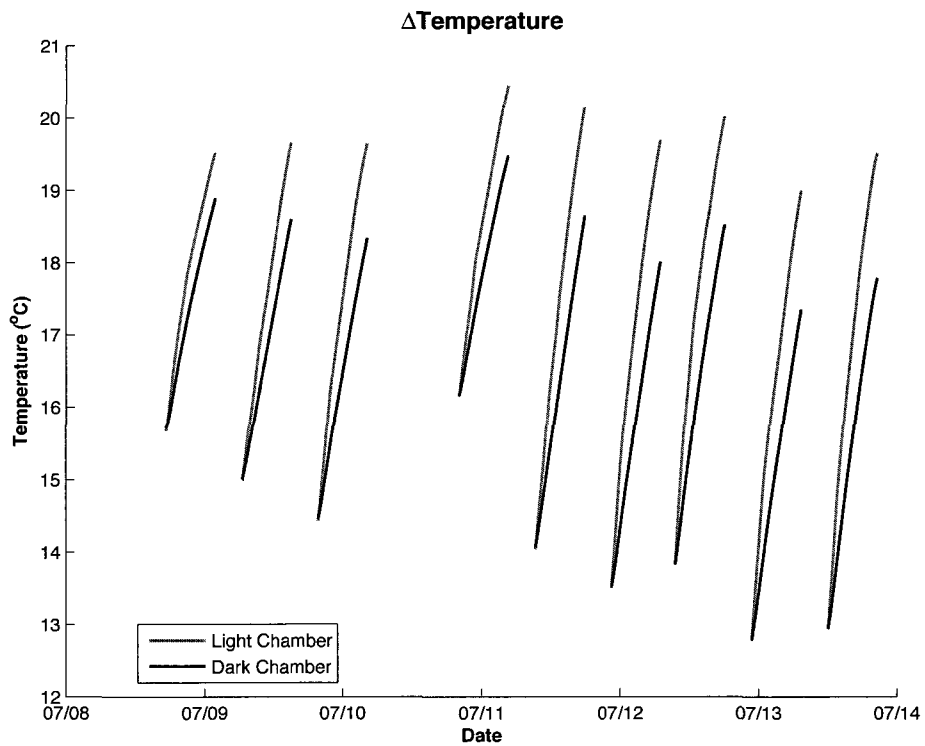


Figure 3-12: This figure shows the temperature of the water in each chamber during a series of 9 incubations where questionable respiration data was collected.

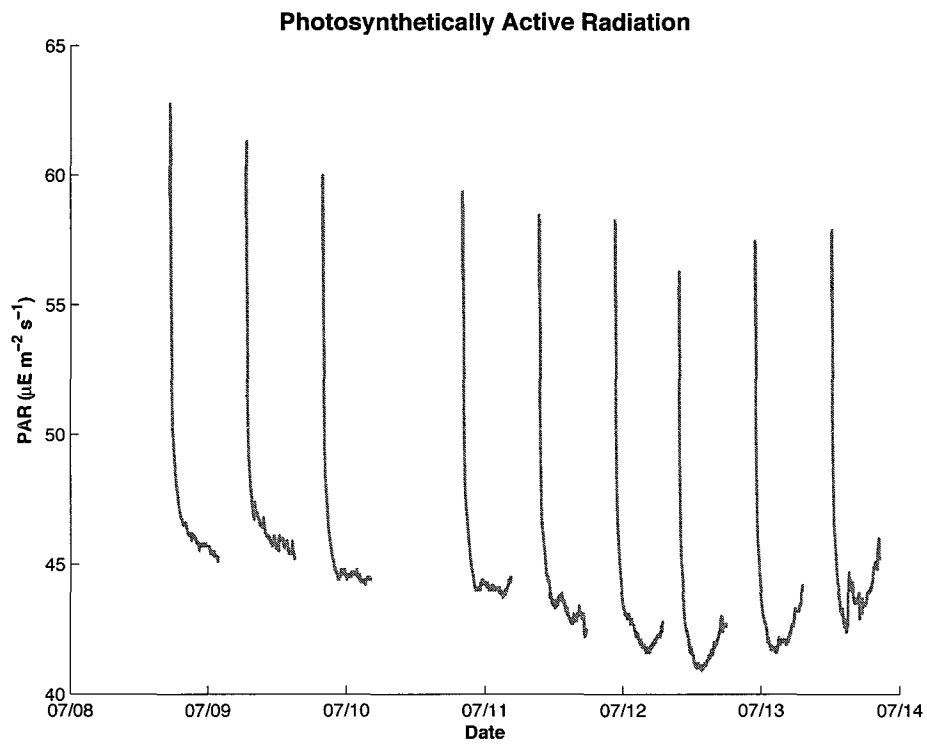


Figure 3-13: This figure shows PAR during a series of 9 incubations where suspect respiration data was collected. The red area highlights questionable PAR data.

GPP, Respiration, and NCP

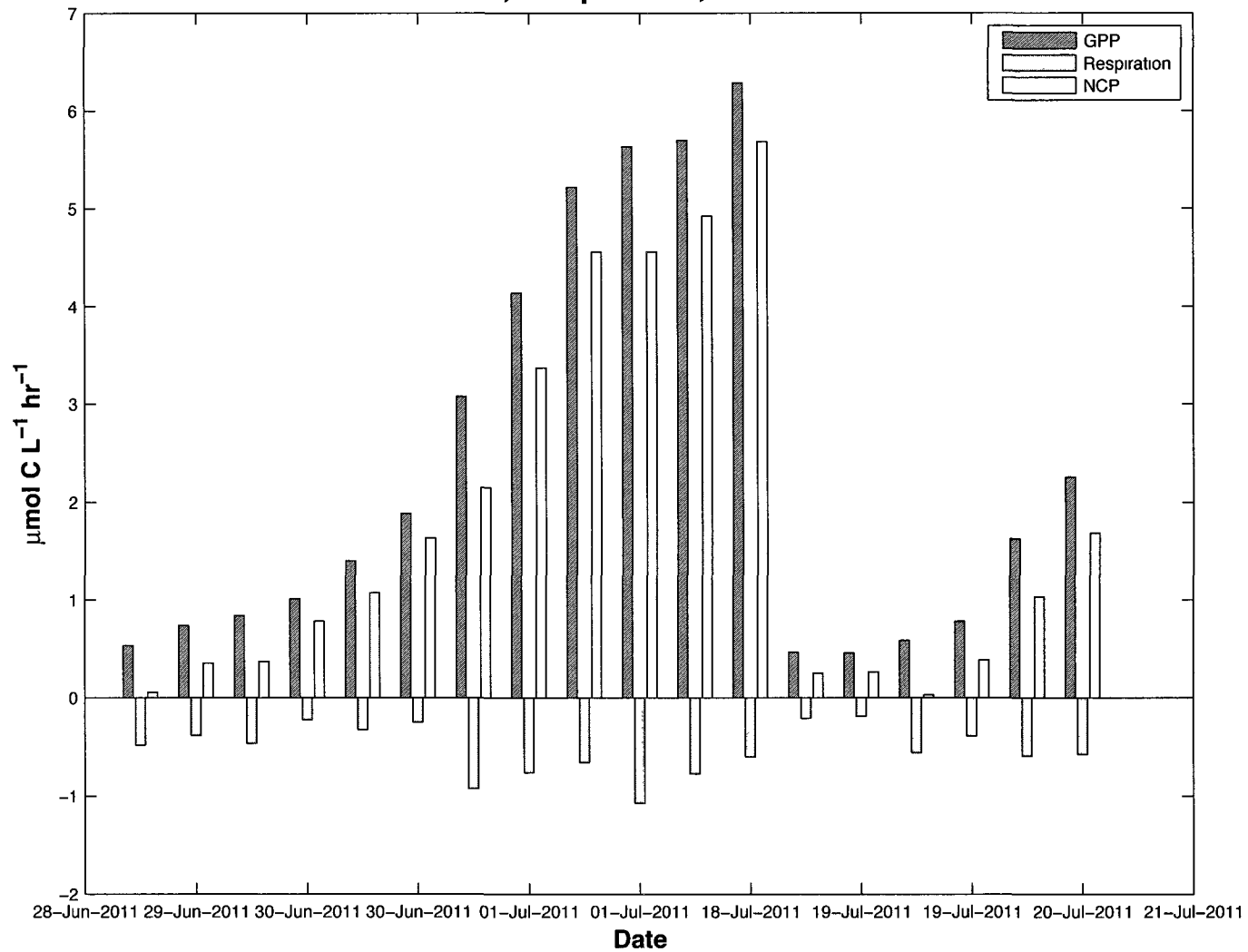


Figure 3-14: This histogram displays gross primary productivity, respiration, and net community productivity for a series of summer incubations from June 28, 2011 to July 21, 2011. Oxygen data has been converted to units of carbon using the Redfield Ratio.

CHAPTER 4

CONCLUSION

A drifter study was conducted in the western Gulf of Maine where the evolution of a water mass and its properties were observed on seven cruises. NCP was calculated as the temporal derivative of the integrated biological oxygen anomaly. Results showed that NCP ranged from apparent autotrophic to heterotrophic conditions, but overall suggest that the western GoM was near equilibrium at the time of this study. NCP values were further compared to changes in POC inventory as estimated from chl-*a*, c_p , and b_{bp} . Integrated POC rates estimated from chl-*a* were found to provide the weakest relationship to NCP while those estimated from c_p and b_{bp} were both robust proxies. $NCP_{OC}(c_p)$ was slightly better correlated likely due to its closer association with the phytoplankton size distribution, whereas $NCP_{OC}(b_{bp})$ can be more affected by non-algal particles at the submicron level.

The second experiment employed a novel light and dark incubation instrument custom-built by Langdon Enterprises to measure NCP and respiration in the Piscataqua Estuary Inlet. Data from the instrument fell into three patterns: expected NCP/respiration rates, no production in the light chamber, and production in the dark chamber. Lack of production was probably due to clogging and biofouling in the pipes providing seawater to the chamber. Production in the dark chamber may have been the result of light leakage, air-sea flux, or hydrogen peroxide production. Overall, expected NCP and respiration rates correlated well to the literature supporting the use of this instrument in future experiments.

It is expected that future NCP studies can benefit from this work. It is hoped that c_p will soon become a satellite ocean color product that could be used to aid

in the quantification of global NCP. This knowledge could further enhance our comprehension of the current global carbon budget, which remains poorly understood. Additionally, it is hoped that the use of this novel automated incubation system will make the study of regional NCP more economically feasible and provide long-term daytime and nighttime NCP and respiration data sets, which are lacking and cannot be easily obtained through ship-board observations.

REFERENCES

- Allison, D. B., Stramski, D., Mitchell, B. G., 2010. Empirical ocean color algorithms for estimating particulate organic carbon in the Southern Ocean. *Journal of Geophysical Research* 115, C10044, doi:10.1029/2009JC006040.
- Álvarez, M., Ríos, A. F., Rosón, G., 2002. Spatio-temporal variability of air-sea fluxes of carbon dioxide and oxygen in the Bransfield and Gerlache Straits during Austral summer 1995/96. *Deep-Sea Research II* 49, 643–662.
- Antoine, D., André, J.-M., Morel, A., 1996. Oceanic primary production 2. estimation at global scale from satellite (coastal zone color scanner) chlorophyll. *Global Biogeochemical Cycles* 10 (1), 57–69.
- Antoine, D., Siegel, D. A., Kostadinov, T., Maritorena, S., Nelson, N. B., Gentili, B., Vellucci, V., Guillocheau, N., 2011. Variability in optical particle backscattering in contrasting bio-optical oceanic regimes. *Limnology and Oceanography* 56 (3), 955–973.
- Behrenfeld, M. J., Boss, E., 2003. The beam attenuation to chlorophyll ratio: an optical index of phytoplankton physiology in the surface ocean? *Deep-Sea Research I* 50, 1537–1549.
- Behrenfeld, M. J., Boss, E., Siegel, D. A., Shea, D. M., 2005. Carbon-based ocean productivity and phytoplankton physiology from space. *Global Biogeochemical Cycles* 19 (GB1006), doi:10.1029/2004GB002299.
- Behrenfeld, M. J., Falkowski, P. G., 1997. A consumer's guide to phytoplankton primary productivity models. *Limnology and Oceanography* 42 (7), 1479–1491.
- Benitez-Nelson, C. R., Buesseler, K. N., Crossin, G., 2000. Upper ocean carbon export, horizontal transport, and vertical eddy diffusivity in the southwestern Gulf of Maine. *Continental Shelf Research* 20, 707–736.
- Bilgili, A., Proehl, J. A., Lynch, D. R., Smith, K. W., Swift, M. R., 2005. Estuary/ocean exchange and tidal mixing in a Gulf of Maine Estuary: A Lagrangian modeling study. *Estuarine, Coastal and Shelf Science* 65 (4), 607–624.
- Bishop, J. K. B., 1999. Transmissometer measurement of POC. *Deep-Sea Research I* 46, 353–369.

- Bishop, J. K. B., Calvert, S. E., Soon, M. Y. S., 1999. Spatial and temporal variability of POC in the northeast Subarctic Pacific. *Deep-Sea Research II* 46, 2699–2733.
- Bjørnsen, P. K., 1988. Phytoplankton exudation of organic matter: Why do healthy cells do it? *Limnology and Oceanography* 33 (1), 151–154.
- Borges, A. V., 2011. *Oceans and the Atmospheric Carbon Content*. Springer, Ch. Present Day Carbon Dioxide Fluxes in the Coastal Ocean and Possible Feedbacks Under Global Change, pp. 47–63.
- Borges, A. V., Delille, B., Frankignoulle, M., 2005. Budgeting sinks and sources of CO₂ in the coastal ocean: Diversity of ecosystems counts. *Geophysical Research Letters* 32 (14), L14601, doi:10.1029/2005GL023053.
- Borges, A. V., Frankignoulle, M., 2002. Distribution of surface carbon dioxide and air-sea exchange in the upwelling system off the Galician coast. *Global Biogeochemical Cycles* 16 (2), 1020, 10.1029/2000GB001385.
- Borges, A. V., Ruddick, K., Schiettecatte, L.-S., Delille, B., 2008. Net ecosystem production and carbon dioxide fluxes in the Scheldt estuarine plume. *BMC Ecology* 8 (15), doi:10.1186/1472-6785-8-15.
- Bricaud, A., Claustre, H., Ras, J., Oubelkheir, K., 2004. Natural variability of phytoplanktonic absorption in oceanic waters: Influence of the size structure of algal populations. *Journal of Geophysical Research* 109, C11010, doi:10.1029/2004JC002419.
- Bricaud, A., Morel, A., Prieur, L., 1981. Absorption by dissolved matter of the sea (yellow substance) in the UV and visible domains. *Limnology and Oceanography* 26 (1), 43–53.
- Brown, T., 2006. Non-reactive gas dynamics in the Piscataqua Estuary Inlet. Master's thesis, University of New Hampshire.
- Buck, K. R., Chavez, F. P., Campbell, L., 1996. Basin-wide distributions of living carbon components and the inverted trophic pyramid of the central gyre of the North Atlantic Ocean, summer 1993. *Aquatic Microbial Ecology* 10, 283–298.
- Caffrey, J. M., 2003. Production, respiration and net ecosystem metabolism in US estuaries. *Environmental Monitoring and Assessment* 81 (1-3), 207–219.
- Caffrey, J. M., 2004. Factors controlling net ecosystem metabolism in US estuaries. *Estuaries* 27 (1), 90–101.
- Caffrey, J. M., Cloern, J. E., Grenz, C., 1998. Changes in production and respiration during a spring phytoplankton bloom in San Francisco Bay, California, USA: implications for net ecosystem metabolism. *Marine Ecology Progress Series* 172, 1–12.

- Cai, W. J., Dai, M. H., Wang, Y. C., 2006. Air-sea exchange of carbon dioxide in ocean margins: A province-based synthesis. *Geophysical Research Letters* 33 (12), L12603, doi:10.1029/2006GL026219.
- Cai, W. J., Wang, Z. H. A., Wang, Y. C., 2003. The role of marsh-dominated heterotrophic continental margins in transport of CO₂ between the atmosphere, the land-sea interface and the ocean. *Geophysical Research Letters* 30 (16), 1849.
- Ciotti, A. M., Lewis, M. R., Cullen, J. J., 2002. Assessment of the relationships between dominant cell size in natural phytoplankton communities and the spectral shape of the absorption coefficient. *Limnology and Oceanography* 47 (2), 404–417.
- de Boyer Montégut, C., Madec, G., Fischer, A. S., Lazar, A., Iudicone, D., 2004. Mixed layer depth over the global ocean: An examination of profile data and a profile-based climatology. *Journal of Geophysical Research* 109 (C12003), doi:10.1029/2004JC002378.
- Dugdale, R. C., Wallace, J. Z., 1960. Light and dark bottle experiments in Alaska. *Limnology and Oceanography* 5, 230–231.
- Durand, M. D., Olson, R. J., 1996. Contributions of phytoplankton light scattering and cell concentration changes to diel variations in beam attenuation in the equatorial Pacific from flow cytometric measurements of pico-, ultra- and nanoplankton. *Deep-Sea Research II* 43 (4-6), 891–906.
- Emerson, S., Hedges, J. I., 2008. *Chemical Oceanography and the Carbon Cycle*, 2nd Edition. Cambridge Univ. Press, Cambridge, UK.
- Falkowski, P., Laws, E., Barber, R., Murray, J., 2003. *Ocean biogeochemistry: The role of the ocean carbon cycle in global change*. Springer, Ch. Phytoplankton and their role in primary, new, and export production, pp. 99–121.
- Falkowski, P., Raven, J., 2007. *Aquatic photosynthesis*, 2nd Edition. Princeton.
- Fischer, G., Karakaş, G., 2009. Sinking rates and ballast composition of particles in the Atlantic Ocean: implications for the organic carbon fluxes to the deep ocean. *Biogeosciences* 6, 85–102.
- Fofonoff, N. P., Millard, R. C. J., 1983. Algorithms for computation of fundamental properties of seawater. *Unesco Technical Papers in Marine Science* (44), 53 pp.
- Fogg, G. E., 1983. The ecological significance of extracellular products of phytoplankton photosynthesis. *Botanica Marina* 26 (1), 3–14.
- Fourqurean, J. W., Webb, K. L., Hollibaugh, J. T., Smith, S. V., 1997. Contributions of the plankton community to ecosystem respiration, Tomales Bay, California. *Estuarine, Coastal and Shelf Science* 44, 493–505.

- Frankignoulle, M., Abril, G., Borges, A., Bourge, I., Canon, C., Delille, B., Libert, E., Théate, J.-M., 1998. Carbon dioxide emission from European estuaries. *Science* 282 (5388), 434–436.
- Gaarder, T., Gran, H. H., 1927. Investigations of the production of plankton in the Oslo Fjord. *Rapports et Proces-verbaux des Reunions. Conseil International pour l'exploration de la Mer* 42, 3–48.
- Gardner, W. D., Walsh, I. D., Richardson, M. J., 1993. Biophysical forcing of particle production and distribution during a spring bloom in the North Atlantic. *Deep-Sea Research II* 40 (1/2), 171–195.
- Gattuso, J. P., Pichon, M., Delesalle, B., Frankignoulle, M., 1993. Community metabolism and air-sea CO₂ fluxes in a coral-reef ecosystem (Moorea, French-Polynesia). *Marine Ecology-Progress Series* 96 (3), 259–267.
- Gazeau, F., Borges, A. V., Barron, C., Duarte, C. M., Iversen, N., Middelburg, J. J., Delille, B., Pizay, M. D., Frankignoulle, M., Gattuso, J. P., 2005. Net ecosystem metabolism in a micro-tidal estuary (Randers Fjord, Denmark): evaluation of methods. *Marine Ecology-Progress Series* 301, 23–41.
- Goebel, N. L., Kremer, J. N., 2007. Temporal and spatial variability of photosynthetic parameters and community respiration in Long Island Sound. *Marine Ecology Progress Series* 329, 23–42.
- Green, R. E., Sosik, H. M., Olson, R. J., 2003. Contributions of phytoplankton and other particles to inherent optical properties in New England continental shelf waters. *Limnology and Oceanography* 48 (6), 2377–2391.
- Hamme, R. C., Emerson, S. R., 2006. Constraining bubble dynamics and mixing with dissolved gases: Implications for productivity measurements by oxygen mass balance. *Journal of Marine Research* 64, 73–95.
- Hitchcock, G. L., Kirkpatrick, G., Minnett, P., Palubok, V., 2010. Net community production and dark community respiration in a *Karenia brevis* (Davis) bloom in West Florida coastal waters, USA. *Harmful Algae* 9, 351–358.
- Hopkinson, Jr, C. S., Vallino, J. J., 1995. The relationships among man's activities in watersheds and estuaries: A model of runoff effects on patterns of estuarine community metabolism. *Estuaries* 18 (4), 598–621.
- Jiang, L.-Q., Cai, W.-J., Wang, Y., Diaz, J., Yager, P. L., Hu, X., 2010. Pelagic community respiration on the continental shelf off Georgia, USA. *Biogeochemistry* 98, 101–113.
- Jiang, L.-Q., Cai, W.-J., Wanninkhof, R., Wang, Y., Lüger, H., 2008. Air-sea CO₂ fluxes on the U.S. South Atlantic Bight: Spatial and seasonal variability. *Journal of Geophysical Research* 113 (C07019), doi:10.1029/2007JC004366.

- Jin, X., Najjar, R. G., Louanchi, F., Doney, S. C., 2007. A modeling study of the seasonal oxygen budget of the global ocean. *Journal of Geophysical Research* 112 (C5), C05017, doi:10.1029/2006JC003731.
- Johnson, K. S., Pytkowicz, R. M., 1979. Biological production and the exchange of oxygen and carbon dioxide across the sea surface in Stuart Channel, British Columbia. *Limnology and Oceanography* 24 (3), 474–482.
- Jönsson, B. F., Salisbury, J. E., Mahadevan, A., 2010. Large variability in continental shelf production of phytoplankton carbon revealed by satellite. *Biogeosciences Discussions* 7, 8953–8978.
- Kemp, W. M., Boynton, W. R., 1980. Influence of biological and physical processes on dissolved oxygen dynamics in an estuarine system: Implications for measurement of community metabolism. *Estuarine and Coastal Marine Science* 11, 407–431.
- Kirk, J. T. O., 1994. *Light and Photosynthesis in Aquatic Ecosystems*, 2nd Edition. Cambridge.
- Knap, A., Michaels, A., Close, A., Ducklow, H., Dickson, A., (Eds.), 1996. *Protocols for the Joint Global Ocean Flux Study (JGOFS) Core Measurements*. JGOFS Report Nr. 19, vi+170 pp. Reprint of the IOC Manuals and Guides No. 29, UNESCO 1994.
- Kortzinger, A., 2003. A significant CO₂ sink in the tropical Atlantic Ocean associated with the Amazon River plume. *Geophysical Research Letters* 30 (24), 2287.
- Kudryavtsev, V. N., Soloviev, A. V., 1990. Slippery near-surface layer of the ocean arising due to daytime solar heating. *Journal of Physical Oceanography* 20 (5), 617–628.
- Langdon, C., 1987. On the causes of interspecific differences in the growth-irradiance relationship for phytoplankton. Part 1. A comparative study of the growth-irradiance relationship of three marine phytoplankton species: *Skeletonema costatum*, *Olisthodiscus luteus* and *Gonyaulax tamarensis*. *Journal of Plankton Research* 9 (3), 459–482.
- Lee, K., 2001. Global net community production estimated from the annual cycle of surface water total dissolved inorganic carbon. *Limnology and Oceanography* 46 (6), 1287–1297.
- Libes, S., 1992. *An Introduction to Marine Biogeochemistry*, 1st Edition. Wiley.
- Liss, P., Merlivat, L., 1986. The role of air-sea exchange in geochemical cycling. Springer, Ch. Air-sea gas exchange rates: Introduction and synthesis, pp. 113–128.
- Loisel, H., Bosc, E., Stramski, D., Oubelkheir, K., Deschamps, P.-Y., 2001. Seasonal variability of the backscattering coefficient in the Mediterranean Sea based on Satellite SeaWiFS imagery. *Geophysical Research Letters* 28 (22), 4203–4206.

- Mague, T. H., Friberg, E., Hughes, D. J., Morris, I., 1980. Extracellular release of carbon by marine phytoplankton; a physiological approach. *Limnology and Oceanography* 25 (2), 262–279.
- Marañón, E., Cermeño, P., Fernández, E., Rodríguez, J., Zabala, L., 2004. Significance and mechanisms of photosynthetic production of dissolved organic carbon in a coastal eutrophic ecosystem. *Limnology and Oceanography* 49 (5), 1652–1666.
- Marra, J., 2002. Phytoplankton productivity: Carbon assimilation in marine and freshwater ecosystems. Blackwell, Ch. Approaches to the measurement of plankton production, pp. 78–108.
- Marra, J., Langdon, C., Knudson, C. A., 1995. Primary production, water column changes, and the demise of a *Phaeocystis* bloom at the Marine Light-Mixed Layers site (59°N, 21°W) in the northeast Atlantic Ocean. *Journal of Geophysical Research* 100 (C4), 6633–6643.
- Martz, T. R., DeGrandpre, M. D., Strutton, P. G., McGillis, W. R., Drennan, W. M., 2009. Sea surface pCO₂ and carbon export during the Labrador Sea spring-summer bloom: An in situ mass balance approach. *Journal of Geophysical Research* 114 (C09008).
- McCardell, G., O'Donnell, J., 2009. A novel method for estimating vertical eddy diffusivities using diurnal signals with application to western Long Island Sound. *Journal of Marine Systems* 77, 397–408.
- McNeil, C. L., Katz, D. R., Ward, B., McGillis, W. R., Johnson, B. D., 2006a. A method to estimate net community metabolism from profiles of dissolved O₂ and N₂. *Hydrobiologia* 571, 181–190.
- McNeil, C. L., Ward, B., McGillis, W. R., DeGrandpre, M. D., Marcinowski, L., 2006b. Fluxes of N₂, O₂, and CO₂ in nearshore waters off Martha's Vineyard. *Continental Shelf Research* 26, 1281–1294.
- Mishonov, A. V., Gardner, W. D., Richardson, M. J., 2003. Remote sensing and surface POC concentration in the South Atlantic. *Deep-Sea Research II* 50, 2997–3015.
- Moffett, J. W., Zafiriou, O. C., 1990. An investigation of hydrogen peroxide chemistry in surface waters of Vineyard Sound with H₂¹⁸O₂ and ¹⁸O₂. *Limnology and Oceanography* 35 (6), 1221–1229.
- Najjar, R. G., Keeling, R. F., 2000. Mean annual cycle of the air-sea oxygen flux: A global view. *Global Biogeochemical Cycles* 14 (2), 573–584.
- Nicholson, D., Emerson, S., Khatiwala, S., Hamme, R. C., In Press. Proceedings on the 6th International Symposium on Gas Transfer at Water Surfaces. Kyoto Univ. Press, Ch. An inverse approach to estimate bubble-mediated air-sea gas flux from inert gas measurements.

- Nightingale, P. D., Malin, G., Law, C. S., Watson, A. J., Liss, P. S., Liddicoat, M. I., Boutin, J., Upstill-Goddard, R. C., 2000. In situ evaluation of air-sea gas exchange parameterizations using novel conservative and volatile tracers. *Global Biogeochemical Cycles* 14 (1), 373–387.
- Odum, H. T., 1956. Primary production in flowing waters. *Limnology and Oceanography* 1 (2), 102–117.
- Packard, T. T., Christensen, J. P., 2004. Respiration and vertical carbon flux in the Gulf of Maine water column. *Journal of Marine Research* 62, 93–115.
- Palenik, B., Morel, F. M. M., 1988. Dark production of H₂O₂ in the Sargasso Sea. *Limnology and Oceanography* 33 (6), 1606–1611.
- Palenik, B., Zafiriou, O. C., Morel, F. M. M., 1987. Hydrogen peroxide production by a marine phytoplankter. *Limnology and Oceanography* 32 (6), 1365–1369.
- Pamatmat, M. M., 1997. Non-photosynthetic oxygen production and non-respiratory oxygen uptake in the dark: a theory of oxygen dynamics in plankton communities. *Marine Biology* 129, 735–746.
- Prowe, A. E. F., Thomas, H., Patsch, J., Kuhn, W., Bozec, Y., Schiettecatte, L.-S., Borges, A. V., deBaar, H. J. W., 2009. Mechanisms controlling the air-sea CO₂ flux in the North Sea. *Continental Shelf Research* 29, 1801–1808.
- Redfield, A. C., 1948. The exchange of oxygen across the sea surface. *Journal of Marine Research* 7, 347–361.
- Riley, G. A., 1941. Plankton studies. IV. Long Island Sound. *Bull Bingham Oceanography Collection* 7, 1–93.
- Roesler, C., Boss, E., 2003. The beam attenuation to chlorophyll ratio: an optical index of phytoplankton physiology in the surface ocean? *Geophysical Research Letters* 30 (9).
- Russell, M. J., Montagna, P. A., 2007. Spatial and temporal variability and drivers of net ecosystem metabolism in western Gulf of Mexico estuaries. *Estuaries and Coasts* 30 (1), 137–153.
- Sambrotto, R. N., Langdon, C., 1994. Water column dynamics of dissolved inorganic carbon (DIC), nitrogen and O₂ on Georges Bank during April, 1990. *Continental Shelf Research* 14 (7/8), 765–789.
- Sharqawy, M. H., Lienhard, J. H., Zubair, S. M., 2010. Thermophysical properties of seawater: a review of existing correlations and data. *Desalination and Water Treatment* 16, 354–380.
- Silker, W. B., 1972. Horizontal and vertical distributions of radionuclides in the north Pacific Ocean. *Journal of Geophysical Research* 77, 1061–1070.

- Smith, S. D., 1988. Coefficients for sea surface wind stress, heat flux, and wind profiles as a function of wind speed and temperature. *Journal of Geophysical Research* 93 (C12), 15,467–15,472, doi:10.1029/JC093iC12p15467.
- Smith, S. V., Marsh, J. A., 1973. Organic carbon production on windward reef flat of Eniwetok-Atoll. *Limnology and Oceanography* 18 (6), 953–961.
- Spitzer, W. S., Jenkins, W. J., 1989. Rates of vertical mixing, gas exchange and new production: Estimates from seasonal gas cycles in the upper ocean near Bermuda. *Journal of Marine Research* 47, 169–196.
- Steemann-Nielsen, E., 1952. The use of radioactive carbon (C14) for measuring organic production in the sea. *Journal du Conseil International pour l'Exploration de la Mer* 18, 117–140.
- Stefánsson, U., Thórdardóttir, T., Ólafsson, J., 1987. Comparison of seasonal oxygen cycles and primary production in the Faxaflói region, southwest Iceland. *Deep-Sea Research* 34 (5/6), 725–739.
- Stramski, D., Boss, E., Bogucki, D., Voss, K. J., 2004. The role of seawater constituents in light backscattering in the ocean. *Progress in Oceanography* 61 (1), 27–56.
- Stramski, D., Kiefer, D. A., 2001. Light scattering by microorganisms in the open ocean. *Progress in Oceanography* 28 (4), doi:10.1016/0079-6611(91)90032-H.
- Stramski, D., Reynolds, R. A., Kahru, M., Mitchell, B. G., 1999. Estimation of particulate organic carbon in the ocean from satellite remote sensing. *Science* 285, 239–242.
- Thomas, H., Bozec, Y., Elkalay, K., de Baar, H., 2004. Enhanced open ocean storage of CO₂ from shelf sea pumping. *Science* 304, 953–961.
- Townsend, D. W., 1991. Influences of oceanographic processes on the biological productivity of the Gulf of Maine. *Reviews in Aquatic Sciences* 5 (3-4), 211–230.
- Townsend, D. W., 1998. Sources and cycling of nitrogen in the Gulf of Maine. *Journal of Marine Systems* 16 (3-4), 283–295.
- Townsend, D. W., 2002. An overview of oceanography and biological productivity in the Gulf of Maine. *The Gulf of Maine-NOAA Coastal Ocean Program Regional Synthesis Series* 1, 5–26.
- Townsend, D. W., Christensen, J. P., Stevenson, D. K., Graham, J. J., Chenoweth, S. B., 1987. The importance of a plume of tidally-mixed water to the biological oceanography of the Gulf of Maine. *Journal of Marine Research* 45 (3), 699–728.
- Townsend, D. W., Thomas, A. C., Mayer, L. M., Thomas, M., Quinlan, J., 2006. *The Sea*. Vol. 14. Harvard, Ch. Oceanography of the Northwest Atlantic Continental Shelf, pp. 119–168.

- Ulloa, O., Sathyendranath, S., Platt, T., 1994. Effect of the particle-size distribution on the backscattering ratio in seawater. *Applied Optics* 33 (30), 7070–7077.
- Van Baalen, C., Marler, J. E., 1966. Occurrence of hydrogen peroxide in sea water. *Nature* 211, 951.
- Vandemark, D., Salisbury, J. E., Hunt, C. W., Shellito, S. M., Irish, J. D., McGillis, W. R., Sabine, C. L., Maenner, S. M., 2011. Temporal and spatial dynamics of CO₂ air-sea flux in the Gulf of Maine. *Journal of Geophysical Research* 116 (C01012), doi:10.1029/2010JC006408.
- Wanninkhof, R., 1992. Relationship between wind-speed and gas-exchange over the ocean. *Journal of Geophysical Research-Oceans* 97 (C5), 7373–7382.
- Wanninkhof, R., McGillis, W. R., 1999. A cubic relationship between air-sea CO₂ exchange and wind speed. *Geophysical Research Letters* 26 (13), 1889–1892.
- Weiss, R. F., 1970. The solubility of nitrogen, oxygen and argon in water and seawater. *Deep-Sea Research* 17, 721–735.